Analytical population dynamics underlying harmful algal blooms triggered by prey avoidance

Jang-Geun Choi[1], Thomas C. Lippmann[2], Elizabeth L. Harvey[3]

[1]Center for Ocean Engineering, University of New Hampshire, Durham, NH, United States

[2]Department of Earth Science, University of New Hampshire, Durham, NH, United States

[3]Department of Biological Sciences, University of New Hampshire, Durham, NH, United States

Correspondence: Jang-Geun Choi (Janggeun.Choi@unh.edu)

Highlights

- Equilibriums of a modified NPZD ecosystem model including two different phytoplankton groups (one with better nutrient uptake ability and the other with better prey avoidance) are analytically found and studied.
- The ecosystem must be sufficiently eutrophic, where total nitrogen exceeds a certain threshold, in order for the phytoplankton group having worse nutrient uptake ability (e.g., harmful algae) to be sustained by the system through prey avoidance.
- The modified NPZD system is fully coupled with a hydrodynamic model and idealized numerical experiments resolving physical transport are conducted.

Abstract

A modified version of the NPZD ecosystem model is used to analytically examine the effects of predation avoidance, a possible mechanism for triggering harmful algal blooms (HAB). To resolve HAB development caused by predation avoidance, an additional phytoplankton functional group is considered, one that has slower nutrient uptake and better predation avoidance characteristics than the non-harmful phytoplankton group used in traditional NPZD models. Because the two phytoplankton groups (one non-harmful and one HAB) compete for only one resource within the same system, steady state (equilibrium) conditions cannot occur without the presence of zooplankton; only the non-harmful phytoplankton group, which defeats the HAB group in the resource competition, can survive in the equilibrium. The presence of sufficient zooplankton effectively acts to replenish the nutrient pool by consuming the non-harmful phytoplankton. When this occurs, two equilibrium states are found: one with both phytoplankton groups coexisting, and one that only includes the HAB group. The condition required for equilibrium is that the total nitrogen within the system should be larger than a threshold determined by model coefficients. The threshold and feasibility of the equilibrium are sensitive to the relative HAB predation avoidance coefficient. If the coefficient is larger than the ratio of net growth rates between the HAB and non-harmful phytoplankton group, the threshold becomes infinite, and an equilibrium is not feasible. The time scale for the system to reach an equilibrium state that includes a HAB group is determined asymptotically. The dependence of a threshold condition as a controlling factor may explain the regime shift of dominant species causing HABs. The ecosystem model is fully implemented into the Regional Ocean Modeling System and applied to an idealized coastal embayment (with depths and geometry taken from San Francisco Bay) to show numerically the dominance of prey avoidance dynamics in a natural

shallow water environment that includes advection and diffusion. The analytical results improve strategies for HAB modeling and provide guidance for setting model coefficients necessary to resolve a HAB event.

1. Introduction

Harmful algal blooms (HABs), usually referred to as red tides, are excessive blooms of mono-phytoplanktonic species that can significantly increase fish mortality and cause large economic loss to fisheries, aquaculture industries, and touristic activities by assimilating toxins and consuming all dissolved oxygen (Jin et al., 2008; Park et al., 2013). Recently, HABs have occurred more frequently due to trends in global warming and increased anthropogenic nutrient input to aquatic systems (Padmakumar et al., 2012; Lee et al., 2013; Griffith and Gobler, 2020). Although many research directions have been pursued to better understand their dynamics, collectively they show that HABs are one of the most complex coastal ecosystem processes that links biogeochemical and hydrodynamical characteristics of the ambient environment (He et al., 2008; Lee, 2008; Li et al., 2009; Kim et al., 2016; Zhou et al., 2017; Baek et al., 2020).

Modeling approaches are frequently used as powerful tools to resolve the complexity of HABs. In many laboratory culturing experiments, single-equation models are simply regressed against measured culturing results (Lee et al., 2001; Cho and Cho, 2014; Lim et al., 2014; Shankar et al., 2014). Adding to the complexity, interactions between HAB groups and other phytoplankton groups including diatoms are common, and can result in a wide variety of outcomes (Kwon et al., 2014; Lim et al., 2014; Oh et al., 2015). Several studies experimentally show that the presence of other phytoplankton groups (e.g., typical non-harmful diatoms) inhibits the growth of several HAB groups (Mitra and Flynn, 2006; Lim et al., 2014). Furthermore, nutrient uptake ability by the HAB group, estimated by laboratory experiments, implies that the HAB group is defeated by the diatoms in the resource competition (Eppley et al., 1969; Lee et al., 2001; Kudela et al., 2010; Cho and Cho, 2014; Oh et al., 2015), and thus plays a primal role in suppressing growth of one phytoplankton group relative to the other (Tilman, 1977).

71 Various mechanisms have been suggested to explain how the HAB group can bloom,
72 including mixotrophic behavior (Jeong et al., 1999; Jeong et al., 2004), swimming ability (Lim et
73 al., 2014; Jeong et al., 2017), allelopathy effects (Fistarol et al., 2004; Tang and Gobler, 2010;
74 Lim et al., 2014), multi-resource competition (Glibert and Burkholder, 2011; Zhou et al., 2017),
75 and prey avoidance (Solé et al., 2006; Mitra and Flynn, 2006; Flynn, 2008; Harvey and Menden-
76 Deuer, 2011 and 2012). The key mechanism triggering a HAB differs by species, but here we
77 focus on details of population dynamics in prey avoidance. Mitra and Flynn (2006) developed a
78 simple ecosystem model that consists of two phytoplankton groups (one HAB and one non-
79 HAB), one nutrient, and one zooplankton species. Their model considered allelopathy, prey
80 switching, and prey rejection of the HAB group, and through sensitivity experiments concluded
81 that prey rejection plays the most important role in the formation of HABs. However, Mitra and
82 Flynn (2006) did not discuss population dynamics of the prey avoidance. In addition, models
83 designed to reconstruct laboratory experiments are difficult to extrapolate to the field. Although
84 previous studies, including Mitra and Flynn (2006), explicitly consider the interactions between
85 HABs and the ambient system using models, most analyses are focused on how well numerical
86 solutions reproduce the observations. Analytical studies for the system of governing equations
87 are generally not considered even though the ecosystem dynamics are determined by the
88 equations.

89 It would be expected that turbulence and the Margalef framework would play an
90 important structuring role in the ecosystem model for pelagic environments (Margalef, 1978;
91 Cullen et al., 2002). However, the purpose of this study is to examine the dynamics of prey
92 avoidance that are not resolved by the Margalef framework, and applicable to well-mixed
93 shallow coastal environments where the water depths are similar in scale to (or shallower than)

pelagic mixed layer depths and the euphotic layer. Based on the Margalef framework, coastal environments with high turbulence (due to tidal mixing) and high nutrient concentration are expected to favor diatom dominance, yet many observations show that non-diatom HABs occur in these shallow eutrophic environments (Wilkerson et al., 2006; Anderson, 2009; Lee et al., 2013; Kang et al., 2015). This implies the presence of dynamics not resolved by the Margalef framework, with prey avoidance as a likely candidate (Mitra and Flynn, 2006; Harvey and Menden-Deuer, 2012; Kang et al., 2015). Our initial model development without consideration of prey avoidance mechanisms (not shown herein) simulated dominant diatoms consistent with not only the Margalef framework but also with the Tilman framework (Tilman, 1977; diatoms having better nutrient uptake ability to defeat HAB groups in resource competition). In the work presented here, we focus on the population dynamics caused by prey avoidance rather than the interaction between phytoplankton growth and turbulence.

In this work, we conduct an analytical analysis of a modified Nutrient-Phytoplankton-Zooplankton-Detritus (NPZD) model that includes a harmful phytoplankton group to study population dynamics of prey avoidance. It should be noted that the model in this study describes the HAB group as a phytoplankton functional group having better predation avoidance in the ecosystem limited by one resource (nitrogen), and thus is designed to highlight the prey avoidance mechanism of the HAB group. In its present form, the model does not consider HABs triggered by unresolved mechanisms (e.g., multi-resource competition or mixotrophic behavior) so cannot be globally applied to HABs problems.

To discuss the dynamics governed by prey-predation interaction between components of the ecosystem, no physical transport is considered and steady-state is assumed in the analytical development. The steady-state solutions (equilibriums) of the modified NPZD model under these

assumptions are found and stability conditions for each equilibrium state are discussed to determine when the HAB group can be sustained in the ecosystem without extinction. Details of the resource competition between two different phytoplankton groups and top-down control mechanisms through prey avoidance are examined and discussed. In addition, the modified NPZD system is fully coupled with a numerical hydrodynamic model where all terms in the general ecological-physical coupled model are retained without the assumptions in the analytical development, and thus temporal rate of change and all transport processes (advection, mixing, and sinking of detritus) for ecological variables are considered. Using the fully coupled model, idealized experiments describing HAB development in an idealized coastal embayment (with depths and geometry taken from San Francisco Bay) are compared with equilibrium states predicted by the theory.

2. Method

2.1. Ecosystem models

In the following, the NPZD system is used as the basis of the marine ecosystem model. The NPZD model consists of four variables (nutrient, phytoplankton, zooplankton, and detritus) and describes the basic cycle of mass (nitrogen) in the marine ecosystem; nutrient is taken up by phytoplankton, phytoplankton are grazed by zooplankton, the plankton become detritus through mortality, and detritus is remineralized. Although there are more sophisticated models, the simple (and widely used) NPZD model contains sufficient complexity to describe many realistic marine ecosystems (Onitsuka et al., 2007; Xu et al., 2008; Perruche et al., 2010; Priester et al., 2017; Cruz-Rico and Rivas, 2018). Furthermore, the NPZD system has been theoretically

scrutinized (Busenberg et al., 1990; Edwards, 2001; Heinle and Slawig, 2013a and 2013b; which are revisited and further discussed in section 3.1), and can be easily modified and expanded to resolve additional ecological dynamics (Newberger et al., 2003; Lima and Doney, 2004; Koné et al., 2005; Fennel et al., 2006; Kishi et al., 2007; Fiechter et al., 2009). Governing equations for the NPZD system are slightly different in each study; equations suggested by Powell et al. (2006) are used in this study because their model is coupled with the publicly available Regional Ocean Modeling System (ROMS; Shchepetkin and McWilliams, 2005) and easily accessible.

To resolve the resource competition and different predation pressure between two specific phytoplankton groups, we include one additional phytoplankton group representing the harmful phytoplankton (HAB group). The purpose is to analytically examine population dynamics of the prey avoidance in the NPZD system by developing an optimal model with enough complexity to resolve prey avoidance in the NPZD system but simple enough to be studied by analytical approaches. The governing equations of our modified NPZD system including a HAB group are given by

$$\frac{dN}{dt} = \delta D + \gamma GZ - U_1 P_1 - U_2 P_2$$

$$\frac{dP_1}{dt} = U_1 P_1 - (1 - \Pi) GZ - \sigma_1 P_1$$

$$\frac{dP_2}{dt} = U_2 P_2 - \Pi GZ - \sigma_2 P_2 \qquad (1)$$

$$\frac{dZ}{dt} = (1 - \gamma) GZ - \xi Z$$

$$\frac{dD}{dt} - \frac{\partial (w_d D)}{\partial z} = \sigma_1 P_1 + \sigma_2 P_2 + \xi Z - \delta D$$

where t is time, and N, P_1, P_2, Z, and D indicate nutrient, normal (non-harmful) phytoplankton, HAB group, zooplankton, and detritus concentrations, respectively. U_1 U_2, G, and Π are growth rates of each phytoplankton group, the zooplankton grazing, and predation probability function, respectively, and defined as

$$U_n(N) = V_n \frac{N}{N + k_n} \frac{\alpha_n I}{\sqrt{{V_n}^2 + (\alpha_n I)^2}}$$

$$G(P_1, P_2) = R_m\left(1 - e^{-\Lambda(P_1 + \psi P_2)}\right)$$

$$\Pi(P_1, P_2) = \frac{\psi P_2}{P_1 + \psi P_2}$$

where subscript *n* takes on values of 1 or 2. The concept of a predation probability function and grazing term is described in Fennel and Neumann (2004) but modified here to consider the different predation pressure induced by each phytoplankton group (Post et al., 2000; Koné et al., 2005; Oguz et al., 2016). The other variables are constant model coefficients (with values given in Table 1). The coefficients shared with traditional NPZD models are the default values (Powell et al., 2006; Fiechter et al., 2009).

Key differences between the traditional NPZD model and the modified NPZD model in this study include the ability to resolve two different phytoplankton groups and the effects of different predation avoidance ability. In the modified NPZD model, two phytoplankton functional groups are considered: the HAB group is defined as the phytoplankton having worse nutrient uptake ability and better predation avoidance ability than the other (non-harmful) phytoplankton group. The model is designed to elucidate the dynamics of top-down control of specific HABs triggered by predation avoidance. The maximum growth rate of P_2 is chosen as a

reasonable value that describes slower nutrient uptake kinetics than that for P_1 ($V_2 < V_1$; Table 1). In this study, the mass transfer between each state variable is defined by nitrogen, and thus the model describes the nitrogen cycle of the ecosystem with the units of the variables and half saturation coefficients given in moles of nitrogen ($\mu M\text{-}N$).

Table 1. Model coefficients of the modified NPZD system.

Coefficient name	symbol	value	Unit
P_1 maximum growth rate	V_1	1.5	1/day
P_1 nitrate half saturation concentration	k_1	1.0	$\mu M\text{-}N$
P_1 natural mortality rate	σ_1	0.1	1/day
P_1 initial slope of P-I curve	α_1	0.025	m^2/W/day
P_1 self-shading coefficient	k_{P_1}	0.0095	1/(m $\mu M\text{-}N$)
P_2 maximum growth rate	V_2	0.4	1/day
P_2 nitrate half saturation concentration	k_2	1.0	$\mu M\text{-}N$
P_2 natural mortality rate	σ_2	0.1	1/day
P_2 initial slope of P-I curve	α_2	0.025	m^2/W/day
P_2 self-shading coefficient	k_{P_2}	0.0095	1/(m $\mu M\text{-}N$)
P_2 relative predation avoidance ability	ψ	0.075	-
Z maximum grazing rate	R_m	0.52	1/day
Z Ivlev constant	Λ	0.84	1/$\mu M\text{-}N$
Z excretion efficiency	γ	0.3	-
Z mortality rate	ξ	0.145	1/day
D remineralization rate	δ	1.03	1/day
D sinking speed	w_d	8.0	m/day
Water light attenuation coefficient	k	0.067	1/m

The parameter ψ is a non-dimensional number that defines the P_2 predation avoidance ability relative to that of P_1. When $\psi < 1$, the zooplankton group prefers to consume P_1 (better predation avoidance of P_2 than P_1), whereas $\psi > 1$ indicates more P_2 preference than P_1. For $\psi = 1$, the zooplankton group has no preference for either phytoplankton group because both groups have identical predation avoidance. The sensitivity of the system on given ψ values is discussed in section 3.2.2. Figure 1 depicts a schematic of the modified NPZD ecosystem model showing the various nitrogen cycling processes, including uptake of nutrients by phytoplankton, grazing by zooplankton, excretion of nutrients from phytoplankton, mortality of phytoplankton and zooplankton, and remineralization of detritus. This model can be considered as a NPPZD type having two different phytoplankton functional groups, P_1 and P_2. Characteristics of each phytoplankton group are identical to those used by Mitra and Flynn (2006), where P_1 has better nutrient uptake ability (represented by $V_2 < V_1$) but P_2 has better predation avoidance ($\psi \ll 1$).

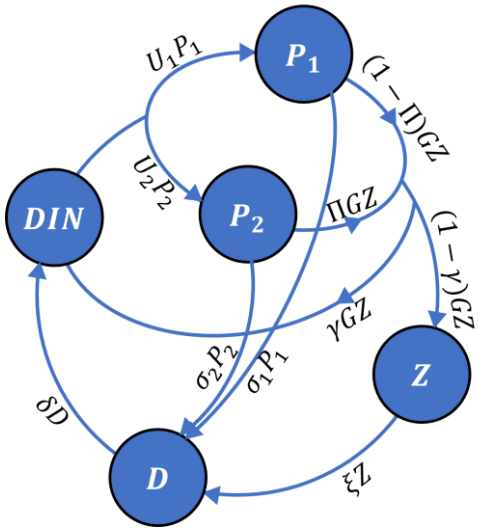

Figure 1. Schematic for the modified NPZD system that resolves an additional phytoplankton group. The normal (non-harmful) phytoplankton group P_1 is described as having better nutrient

uptake ability, and the harmful algal group P_2 is described as having better prey avoidance ability.

2.2. Equilibrium points

Steady-state solutions, ignoring left hand side terms of system (1), are frequently used to analyze characteristics and dynamics of ecosystem models (Tilman, 1977; Newberger et al., 2003; Perruche et al., 2010; Heinle and Slawig, 2013a and b). Although the system (1) is nonlinear, steady-state solutions are easily obtained. Negative or imaginary solutions are non-physical and not discussed further. Because system (1) is closed and conserves mass, the five equations in (1) with steady-state are undetermined. The last equation needed to reach a solution can be obtained by summing all equations in (1) that yields $d(N + P_1 + P_2 + Z + D)/dt = 0$, and can be written as

$$N + P_1 + P_2 + Z + D = N_T$$

where N_T indicates the total nitrogen concentration determined by the sum of all the state variable in initial conditions. The steady-state solutions are expressed as a function of model coefficients (Table 1) and N_T. To represent the state of the system, state variables are denoted as a vector $E^{(m)} = \left(N^{(m)}, P_1^{(m)}, P_2^{(m)}, Z^{(m)}, D^{(m)}\right)$, similar to Heinle and Slawig (2013a), where superscript *m* represents the index of each steady-state solution. The stability condition for each steady-state solution can also be found. For any given initial condition that progresses toward a stable solution, the stability condition will determine the feasibility of that stable solution. The stability condition can be determined by linearization of the ordinary differential equation system

(Heinle and Slawig, 2013a); here we focus on the ecological consequences of the stability condition, similar to Busenberg et al. (1990).

It must be noted that system (1) does not always converge toward a steady-state solution. When total nitrogen in the system is sufficiently high, the steady-state solution changes from a stable focal point towards a neutral stability point where the state of the system oscillates around the steady-state solution (Busenberg et al., 1990). However, the steady-state solution for a neutral stability point attracts the system away from other unstable solutions and remains close to the center of oscillation. In this study, the steady-state solution for a neutral stability point is not discussed further, and the focus is on the transition of stable steady-states from one solution to another, useful for determining the conditions that result in the presence (or absence) of a phytoplankton functional group.

2.3. Numerical experiments

2.3.1. Cross-verification using ordinary differential equation solvers

The equilibriums of the system (1) are cross-verified by numerical solutions based on ordinary differential equation solvers provided by MATLAB. The temporal change terms on the left hand side of (1) are retained in the numerical solutions. System (1) with different ψ and N_T is solved and compared to the theoretical equilibrium. It is worth noting that careful choice of the solver (numerical scheme) and accurate error tolerances are required to obtain a proper numerical solution for highly eutrophic conditions (high N_T) which result in stiff nonlinear oscillations; otherwise, the solvers blow up or reach an equilibrium that disagrees with the theoretical equilibrium (Appendix A). Herein, we use the ode45 solver with both relative and

absolute error tolerances set to 10^{-10}. The ode23t (not shown herein) generates identical results with ode45.

2.3.2. Idealized experiments using ecosystem model fully coupled with hydrodynamics model

To test the theory in a more realistic ecosystem influenced by transport mechanisms, we fully couple system (1) with ROMS and then conduct idealized numerical experiments. Physical transport of ecological variables and detritus sinking are considered in the numerical experiments so both advection and diffusion terms are also considered in the fully coupled model. The model domain for the idealized experiments is chosen based on *Heterosigma akashiwo* blooms in San Francisco Bay that are expected to be triggered by a prey avoidance mechanism (Harvey and Menden-Deuer, 2011). However, it must be noted that the purpose of the idealized experiments is not to accurately simulate HABs of San Francisco Bay, but instead to test dominance of the dynamics elucidated by the equilibriums of system (1) in a more realistic coastal environment that includes physical transport and sinking detritus. The model is designed based on topography from the ETOPO2 dataset (Figure 2) with 10 vertical sigma levels and 500 m lateral spatial resolution. For simplicity, the predominant tide is assumed in the shallow coastal environment and thus the model is forced only by tides (obtained from the TPXO9-atlas tidal dataset available at https://www.tpxo.net/global/tpxo9-atlas) without consideration of wind stress and river discharge. For the mixing, vertical diffusion is resolved by the Mellor-Yamada turbulence closure scheme without lateral diffusion (Mellor and Yamada, 1982). The High-order Spatial Interpolation at the Middle Temporal level (HSIMT; Wu and Zhu, 2010) scheme is chosen to

handle advection of tracers. Although this simple model configuration is not expected to simulate the circulation of the real ocean, we presume that it is sufficiently complex to resolve plausible effects of circulation and mixing of general tide-dominated shallow coastal environments on ecological variables.

For the ecological model configuration, the modified NPZD model is initiated by constant concentration of state variables inside of the bay (Figure 2): all ecological variables are set to 0.1 $\mu M\text{-}N$ except for nutrient concentrations that are set to 1, 4, and 16 $\mu M\text{-}N$ to assess sensitivity to N_T. The concentration of all variables in the offshore region is set to 0 $\mu M\text{-}N$ for simplicity. The ecological model coefficients listed in Table 1 are used and the light intensity is fixed to 158 W/m^2, identical with Powell et al. (2006). In ROMS, the biological sediment option is turned on, which describes sediment remineralization processes and returns nitrogen from the detritus reaching the bottom boundary to the nutrient pool without loss (e.g., denitrification and permanent sedimentation). To examine the role of physical transport, passive tracers are distributed with identical initial conditions as the ecological tracers. The concentration of the passive tracers on the inner shelf is defined as one.

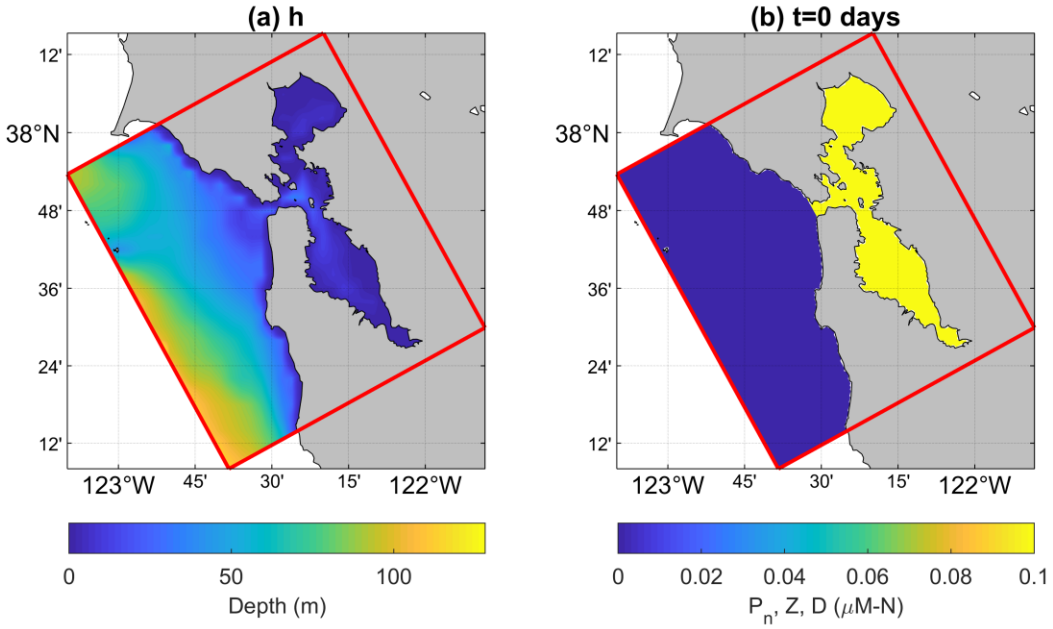

Figure 2. Bathymetry (a) and initial condition of ecological variables (b) in the model domain for the idealized experiments using the ecosystem model fully coupled with ROMS. The initial nutrient concentration is controlled to study sensitivity to total nitrogen N_T.

3. Theory

3.1. Shared solutions with NPZD system ($P_2 = 0$)

Because system (1) converges to the general NPZD model when $P_2 = 0$, steady-state solutions of the general NPZD model are also considered as one of the possible solutions. In this section, equilibriums of the general NPZD model are revisited to highlight the transition of stable solutions (given as total nitrogen levels) and the role of zooplankton in the eutrophic range. The first solution of the general NPZD system requires that all nitrogen in the system exists in nutrient form and all the other state variables are zero, so $E^{(1)} = \left(N^{(1)}, 0,0,0,0\right)$ where $N^{(1)} =$

N_T. This solution occurs when the initial concentration of phytoplankton groups is zero or when nutrient concentrations are not enough to sustain the phytoplankton group, $U_1(N_T) < \sigma_1$, which can be written as

$$N_T < {U_1}^{-1}(\sigma_1) = \frac{\sigma_1 k_1}{V_1 - \sigma_1} \tag{2}$$

where ${U_n}^{-1}(\sigma_n)$ indicates the nutrient concentration that makes the growth rate of the phytoplankton balanced by the mortality rate; in other words, the minimum nutrient concentration needed for the phytoplankton group to be sustained.

A second solution occurs when the zooplankton group does not exist, such that $E^{(2)} = \left(N^{(2)}, P_1^{(2)}, 0, 0, D^{(2)}\right)$. The components of the second equilibrium $E^{(2)}$ are given as

$$N^{(2)} = {U_1}^{-1}(\sigma_1)$$

$$P_1^{(2)} = \frac{\delta}{\delta + \sigma_1}\left(N_T - {U_1}^{-1}(\sigma_1)\right)$$

$$D^{(2)} = \frac{\sigma_1}{\delta + \sigma_1}\left(N_T - {U_1}^{-1}(\sigma_1)\right).$$

This solution is feasible both when zooplankton initially do not exist, or when nutrient concentrations are high enough to sustain the phytoplankton but the phytoplankton concentration itself is not enough to maintain a viable zooplankton population, such that $\sigma_1 < U_1(N_T)$ and $(1-\gamma)G\left(P_1^{(2)}, 0\right) < \xi$. This condition can be written as

$${U_1}^{-1}(\sigma_1) < N_T < {U_1}^{-1}(\sigma_1) + \frac{\delta + \sigma_1}{\delta} P_1^{(3)} \tag{3}$$

where $P_1^{(3)}$ indicates the minimum phytoplankton concentration needed to sustain zooplankton, and corresponds to the phytoplankton concentration that results in a balance between growth and mortality of the zooplankton, and is defined as

$$P_1^{(3)} = G^{-1}\left(\frac{\xi}{1-\gamma}\right) = \frac{1}{\Lambda}\ln\left[\left(1 - \frac{\xi}{R_m(1-\gamma)}\right)^{-1}\right].$$

When the steady-state phytoplankton concentration is enough to sustain zooplankton, or equivalently, the total nitrogen concentration is high enough to sustain both phytoplankton and zooplankton, a third steady-state solution, $E^{(3)} = \left(N^{(3)}, P_1^{(3)}, 0, Z^{(3)}, D^{(3)}\right)$, exists with all non-zero state variables except for P_2. Components of $E^{(3)}$ are determined by

$$N^{(3)^2} + \left(k_1 + V_1 P_1^{(3)}(1-\gamma)\left(\frac{1}{\xi}+\frac{1}{\delta}\right) + \left[P_1^{(3)}\left(1 - \frac{\sigma_1}{\xi}(1-\gamma) + \frac{\sigma_1}{\delta}\gamma\right) - N_T\right]\right) N^{(3)}$$
$$+ \left[P_1^{(3)}\left(1 - \frac{\sigma_1}{\xi}(1-\gamma) + \frac{\sigma_1}{\delta}\gamma\right) - N_T\right] k_1 = 0$$

$$Z^{(3)} = \frac{1-\gamma}{\xi}\left(U_1\left(N^{(3)}\right) - \sigma_1\right) P_1^{(3)}$$

$$D^{(3)} = \frac{1}{\delta}\left((1-\gamma)U_1\left(N^{(3)}\right) + \gamma\sigma_1\right) P_1^{(3)}.$$

It is worth noting that the quadratic equation for $N^{(3)}$ has two solutions, but one is negative and non-physical. $P_1^{(3)}$ is independent of N_T and determined by coefficients related to the zooplankton; all other state variables are dependent on N_T. The condition that allows the zooplankton group to be present is $(1-\gamma)G\left(P_1^{(2)}, 0\right) > \xi$, and can be written as

$$U_1{}^{-1}(\sigma_1) + \frac{\delta}{\delta + \sigma_1} P_1^{(3)} < N_T. \qquad (4)$$

Figure 3 shows components of the steady-state solution to the general NPZD system varying with N_T; that is, feasible steady-state solutions are transited from $E^{(1)}$ to $E^{(2)}$, and $E^{(2)}$ to $E^{(3)}$ whenever N_T becomes higher than the threshold conditions (3) and (4). For $E^{(3)}$, all state variables except for phytoplankton increase with increasing N_T. When N_T is sufficiently high, nutrient concentration $N^{(3)}$ linearly increases, whereas $Z^{(3)}$ and $D^{(3)}$ are saturated and converge to constant values (Figure 3). The solutions $Z^{(3)}$ and $D^{(3)}$ are Monod functions with non-zero intercept. The slope of $N^{(3)}$ and saturated concentration of $Z^{(3)}$ and $D^{(3)}$ can be analytically determined as N_T gets large, and are given in the limit by

$$\lim_{N_T\to\infty} \frac{\partial N^{(3)}}{\partial N_T} = 1$$

$$\lim_{N_T\to\infty} Z^{(3)} = \frac{1-\gamma}{\xi}(V_m - \sigma)P_1^{(3)}$$

$$\lim_{N_T\to\infty} D^{(3)} = \frac{1}{\delta}\big((1-\gamma)V_m + \gamma\sigma\big)P_1^{(3)}.$$

Consequently, in the eutrophic limit, nutrient concentration converges to a linear polynomial function with slope one, and all the other state variables become constant. This implies that once the system is sufficiently eutrophic, additional nitrogen will not influence the steady-state values of phytoplankton, zooplankton, and detritus. Any additional nitrogen is stored in nutrient pools.

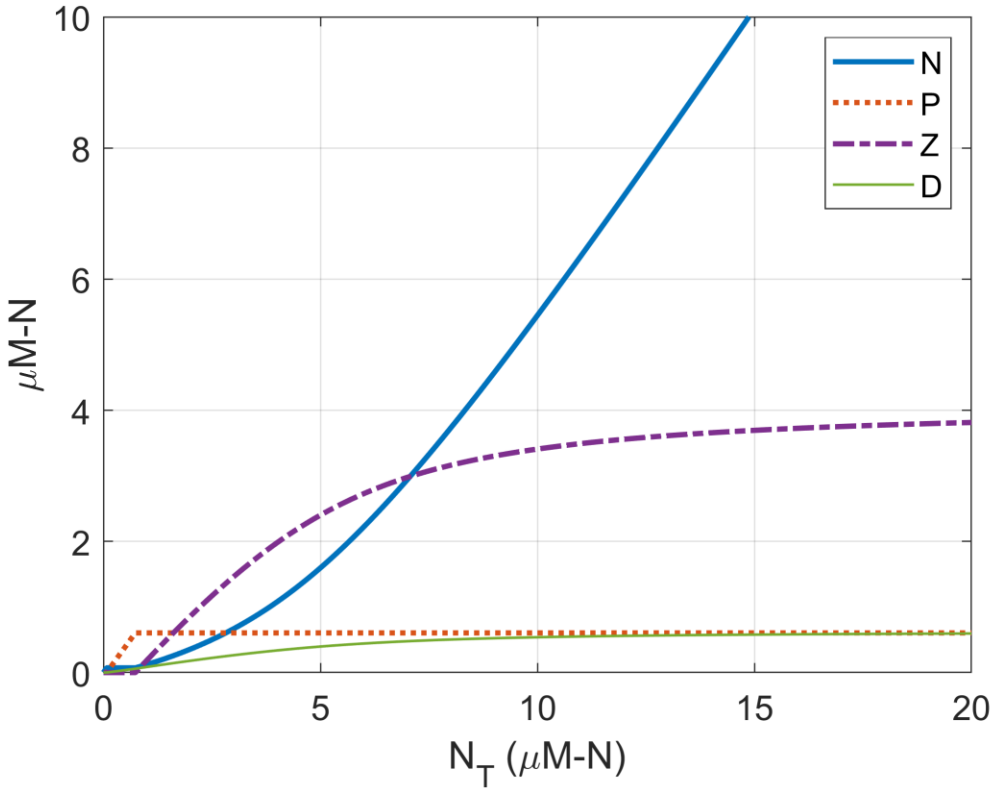

Figure 3. Steady-state solutions of the general NPZD system varying with N_T. In the eutrophic limit, all state variables converge to a constant value except for nutrients which linearly increases with slope one.

The steady-state solutions of the general NPZD system with only one functional phytoplankton group were well discussed by Heinle and Slawig (2013a). The governing equations of NPZD system used by Heinle and Slawig (2013a) were different than those used in this study. In their model, mortality of zooplankton increased nutrient concentration and the inefficiency of zooplankton grazing increased detritus. The opposite occurs in our work where zooplankton mortality increases detritus and the inefficiency of grazing increases nutrient concentration. Regardless, qualitative characteristics of steady-state solutions are the same

because detritus acts as an intermediate state between mortality and remineralization in the closed system, and the presence of a zooplankton group intrinsically plays a role in pumping nitrogen from the phytoplankton pool to the nutrient pool.

3.2. HAB group presence solutions ($P_2 \neq 0$)

3.2.1. Resource competition between two phytoplankton groups without zooplankton ($Z = 0$)

The presence of a HAB group, $P_2 \neq 0$, induces additional steady-state solutions. However, it is worth noting first that steady-state solutions do not exist for situations where P_1 and P_2 coexist without zooplankton ($Z = 0$). This is because system (1) represents two different phytoplankton groups that compete for only one resource (Tilman, 1977). That is, when $P_1 \neq 0$, $P_2 \neq 0$, and $Z = 0$, each governing equation for the phytoplankton groups drives two different steady-state nutrient concentrations, ${U_1}^{-1}(\sigma_1)$ and ${U_2}^{-1}(\sigma_2)$, and thus has no solution. As a result, the phytoplankton group that can survive under conditions with lower nutrient concentration (i.e., lower ${U_n}^{-1}(\sigma_n)$) defeats the other phytoplankton group. The winner of the resource competition is P_1 because of its higher maximum growth rate that contributes to ${U_1}^{-1}(\sigma_1) < {U_2}^{-1}(\sigma_2)$.

There does exist a steady-state solution $E^{(4)} = \left(N^{(4)}, 0, P_2^{(4)}, 0, D^{(4)}\right)$ for which components are given by

$$N^{(4)} = {U_2}^{-1}(\sigma_2)$$

$$P_2^{(4)} = \frac{\delta}{\delta + \sigma_2}\left(N_T - {U_2}^{-1}(\sigma_2)\right)$$

$$D^{(4)} = \frac{\sigma_1}{\delta + \sigma_2}\left(N_T - {U_2}^{-1}(\sigma_2)\right).$$

However, $E^{(4)}$ is sustained by the defeated functional group and represents an unstable saddle point (van Opheusden et al., 2015). The presence of P_1 rapidly moves the state of the system from solution $E^{(4)}$ to $E^{(2)}$. As the state of the system approaches solution $E^{(2)}$, P_2 converges to zero because the growth rate of P_2 around $E^{(2)}$ is less than the mortality, $U_2(N_2) < \sigma_2$, equivalent to ${U_1}^{-1}(\sigma_1) < {U_2}^{-1}(\sigma_2)$. In other words, for the solution $E^{(4)}$ to become viable, the initial concentration of P_1 must be strictly zero. Otherwise, the presence of a minute amount of P_1 moves the state of the system from solution $E^{(4)}$ to $E^{(2)}$. This result is in agreement with many laboratory experiments (Mitra and Flynn, 2006; Lim et al., 2014; Oh et al., 2015; Sukenik and Kaplan, 2021) and indicates that the model system (1) in this study incorporates resource competition dynamics between normal phytoplankton and a HAB group. However, this resource competition does not explain how a HAB group can bloom in the system because P_1 represents non-harmful phytoplankton that are ubiquitous and not likely to be absent in the natural ocean.

3.2.2. Equilibrium with $P_2 \neq 0$

As mentioned above, P_2 cannot exist when zooplankton do not exist because nutrient concentration in the stable steady-state solution contributes to negative net growth rate of the HAB group. However, the presence of zooplankton increases the nutrient concentration as total nitrogen level in the system increases (Figure 3). Once nutrient concentration – increased by

zooplankton – is sufficient to cause larger growth rates than the sum of sink terms (including mortality and predation rate), a steady-state solution with non-zero P_2, $E^{(5)} = \left(N^{(5)}, P_1^{(5)}, P_2^{(5)}, Z^{(5)}, D^{(5)}\right)$, is feasible. The components of solution $E^{(5)}$ are determined by

$$U_2\left(N^{(5)}\right) - \sigma_2 = \psi\left(U_1\left(N^{(5)}\right) - \sigma_1\right)$$

$$Z^{(5)} = \frac{1-\gamma}{\xi}\left(U_1\left(N^{(5)}\right) - \sigma_1\right)P_1^{(3)}$$

$$P_1^{(5)} = \frac{\psi\left(\delta\left(N_T - N^{(5)} - Z^{(5)}\right) - \xi Z^{(5)}\right) - (\sigma_2 + \delta)P_1^{(3)}}{\psi(\sigma_1 + \delta) - (\sigma_2 + \delta)}$$

$$P_2^{(5)} = \frac{\delta\left(N_T - N^{(5)} - Z^{(5)}\right) - \xi Z^{(5)} - (\sigma_2 + \delta)P_1^{(3)}}{(\sigma_1 + \delta) - \psi(\sigma_2 + \delta)}$$

$$D^{(5)} = N_T - N^{(5)} - P_1^{(5)} - P_2^{(5)} - Z^{(5)}.$$

It is worth noting that the first equation above for nutrient concentration can be rewritten in quadratic form with one of the two solutions non-physical, similar to $E^{(3)}$. The condition necessary for $E^{(5)}$ is $U_2\left(N^{(3)}\right) > \sigma_2 + \psi/P_1^{(3)}GZ^{(3)}$, which can be rewritten as $U_2\left(N^{(3)}\right) - \sigma_2 > \psi\left(U_1\left(N^{(3)}\right) - \sigma_1\right)$ and $N^{(3)} > N^{(5)}$. The second form of the condition shows that net growth of P_2 should be larger than that of P_1 weighted by ψ. When P_2 cannot gain sufficient advantage from prey avoidance (sufficiently small ψ), $E^{(5)}$ is unconditionally not possible. Therefore, the coefficient ψ should be sufficiently small for the model to trigger HABs. The maximum ψ which can reach equilibrium with P_2 is also analytically determinable; the former form for the stable condition becomes $V_2 - \sigma_2 > \psi(V_1 - \sigma_1)$ in the eutrophic limit where $N_T \to \infty$ and $N^{(3)} \to \infty$,

so $(V_2 - \sigma_2)/(V_1 - \sigma_1) > \psi$ is required. Because $N^{(3)}$ is a function of N_T, and $N^{(5)}$ is a constant determined by coefficients V_n, k_n, and ψ, the condition necessary for $E^{(5)}$, $N^{(3)} > N^{(5)}$, can be rewritten again as

$$N^{(3)^{-1}}\left(N^{(5)}\right) < N_T \tag{5}$$

showing that N_T must be larger than a threshold determined by coefficients. Explicit form of the thresholds is given in Appendix B. If $\psi > (V_2 - \sigma_2)/(V_1 - \sigma_1)$, conditions for $E^{(5)}$ can never be satisfied, even if $N_T \to \infty$.

When $\psi = 0$, indicating that P_2 is not subject to predation, the complexity of the governing equations (1) is significantly reduced because Π becomes zero, and the steady-state solution $E^{(5)}$ is also simplified. Figure 4 shows the steady-state concentration of each state variable expressed as a function of N_T with $\psi = 0$ and $\psi = 0.075 < (V_2 - \sigma_2)/(V_1 - \sigma_1)$. It is worth noting that solutions of the general NPZD system occur when N_T is less than $N^{(3)^{-1}}\left(N^{(5)}\right)$. Once $\psi = 0$ and N_T is larger than $N^{(3)^{-1}}\left(N^{(5)}\right)$, P_2 and D linearly increase with N_T, and the other state variables become independent of N_T (upper panel of Figure 4). In this case, the dynamics described by the system are straightforward: P_2 that are not consumed by zooplankton take up surplus nutrients converted from P_1 by the zooplankton.

When ψ is sufficiently small and positive so that condition (5) is satisfied, P_2 increases as N_T increases, similar to the case where $\psi = 0$; however, at the same time P_1 slowly decreases (lower panel of Figure 4). Eventually, once N_T is high enough, a steady-state solution occurs without P_1, $E^{(6)} = \left(N^{(6)}, 0, P_2^{(6)}, Z^{(6)}, D^{(6)}\right)$. The components of $E^{(6)}$ are given as

$$P_2^{(6)} = \frac{1}{\psi\Lambda}\ln\left[\left(1 - \frac{\xi}{R_m(1-\gamma)}\right)^{-1}\right]$$

$$N^{(6)^2} + \left(k_2 + V_2 P_2^{(6)}(1-\gamma)\left(\frac{1}{\xi}+\frac{1}{\delta}\right) + \left[P_2^{(6)}\left(1 - \frac{\sigma_2}{\xi}(1-\gamma) + \frac{\sigma_2}{\delta}\gamma\right) - N_T\right]\right) N^{(6)}$$

$$+ \left[P_2^{(6)}\left(1 - \frac{\sigma_2}{\xi}(1-\gamma) + \frac{\sigma_2}{\delta}\gamma\right) - N_T\right] k_2 = 0$$

$$Z^{(6)} = \frac{1-\gamma}{\xi}\left(U_2\left(N^{(6)}\right) - \sigma_2\right) P_2^{(6)}$$

$$D^{(6)} = \frac{1}{\delta}\left((1-\gamma)U_2\left(N^{(6)}\right) + \gamma\sigma_2\right) P_2^{(6)}.$$

400 $E^{(6)}$ has identical mathematical characteristics as $E^{(3)}$; $Z^{(6)}$ and $D^{(6)}$ depend on N_T but are
401 saturated and converge to constant values in the eutrophic limit. On the other hand, $N^{(6)}$ linearly
402 increases with N_T in the limit. The condition necessary for $E^{(6)}$ is the absence of P_1 which occurs
403 when the growth rate of P_1 is less than the sum of sink terms, $U_1\left(N^{(6)}\right) < \sigma_1 + 1/P_1^{(3)} G Z^{(6)}$
404 (where $\psi P_2^{(6)} = P_1^{(3)}$). This condition, similar to condition (5), is given by $\psi\left(U_1\left(N^{(6)}\right) - \sigma_1\right) <$
405 $U_2\left(N^{(6)}\right) - \sigma_2$ and $N^{(5)} < N^{(6)}$, which can be written as

$$N^{(6)^{-1}}\left(N^{(5)}\right) < N_T. \qquad (6)$$

406 This steady-state solution shows that P_1 cannot survive in environments where P_2
407 sustains a large enough zooplankton group. It is interesting that both P_1 and P_2 coexist in the
408 eutrophic limit if P_2 is not subject to predation. Conversely, P_1 is not sustained when predation
409 for P_2 is allowed. This implies that the niche of a functional group must be provided and present
410 within the functional group. When P_2 is not consumed by zooplankton, P_1 has a unique niche
411 that sustains a zooplankton group that is required by P_2. However, once P_2 is available as prey

412 for the zooplankton group, P_2 itself can sustain a zooplankton group even without P_1. As a
413 consequence, the role of P_1 in sustaining a zooplankton group is replaced by P_2 in the eutrophic
414 limit.

415 The predation avoidance coefficient ψ plays a crucial role in the behavior of the
416 equilibrium when $P_2 \neq 0$ (Figure 4). Figure 5 shows the sensitivity of analytically determining
417 thresholds of $E^{(5)}$ and $E^{(6)}$ expressed as function of ψ. If P_2 is not subject to predation ($\psi = 0$),
418 the threshold of $E^{(5)}$, given by ${N^{(3)}}^{-1}\left(N^{(5)}\right)$, becomes minimum. On the other hand, the
419 threshold of $E^{(6)}$, given by ${N^{(6)}}^{-1}\left(N^{(5)}\right)$, increases infinitely as $\psi \to 0$, and thus $E^{(6)}$ cannot be
420 feasible if $\psi = 0$. As before, P_1 is necessary to sustain the zooplankton group that is required by
421 P_2 when $\psi = 0$. As ψ increases, ${N^{(3)}}^{-1}\left(N^{(5)}\right)$ increases and the steady-state concentration of P_2
422 decreases because the predation for P_2 is allowed and acts as a sink of P_2. At the same time
423 ${N^{(6)}}^{-1}\left(N^{(5)}\right)$ decreases because P_2 itself can efficiently sustain zooplankton irrespective of P_1.
424 There is another singularity at $\psi = (V_2 - \sigma_2)/(V_1 - \sigma_1)$ where both ${N^{(3)}}^{-1}\left(N^{(5)}\right)$ and
425 ${N^{(6)}}^{-1}\left(N^{(5)}\right)$ become infinite. In this situation, predation for P_2 is too intense and P_2 cannot gain
426 an advantage as the functional group with better predation avoidance. As a result, P_2 does not
427 exist and only $E^{(3)}$ becomes feasible.

428

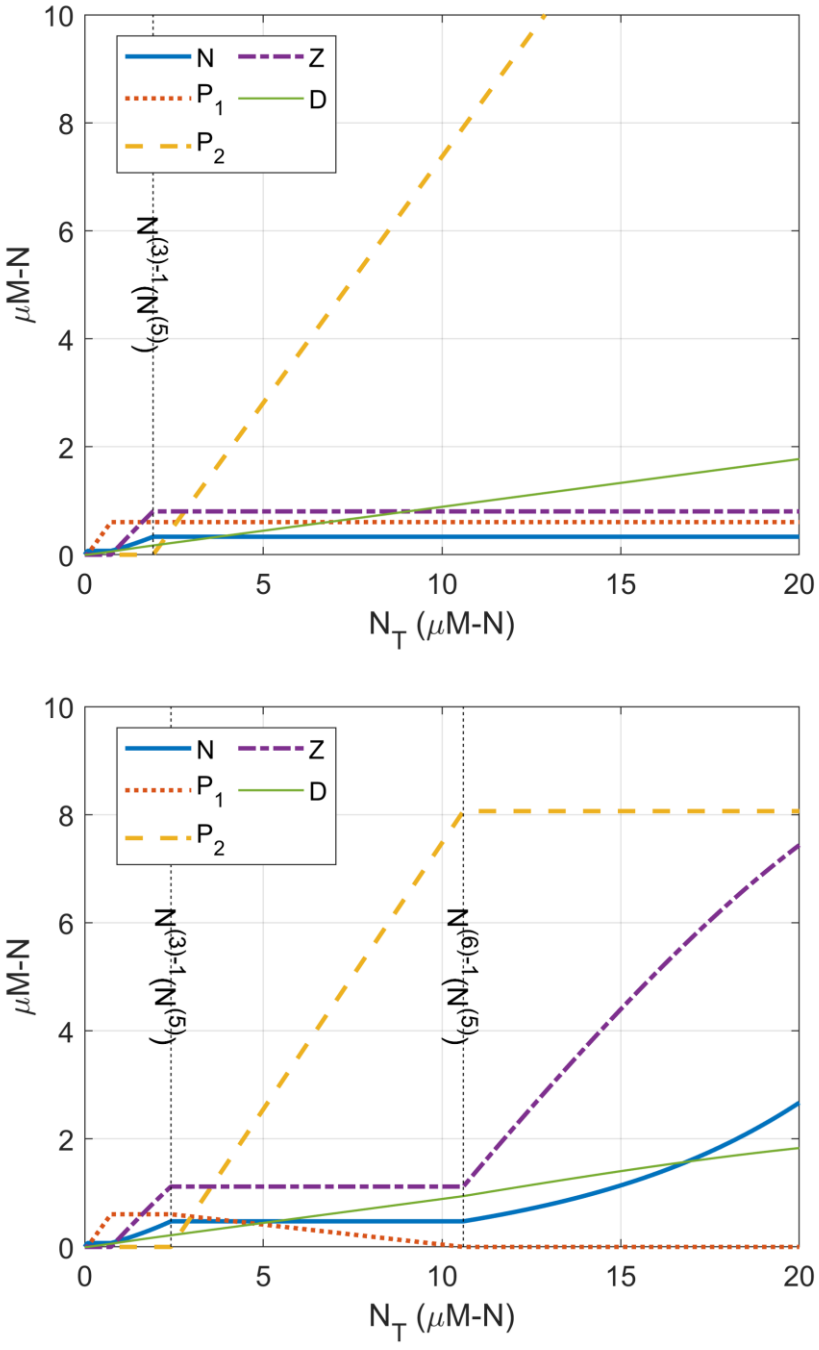

Figure 4. Steady-state solutions of the modified NPZD system with HAB group varying with N_T for the cases $\psi = 0$ (upper panel) and $\psi \neq 0$ (lower panel). Vertical dashed lines indicate thresholds of the equilibriums with $P_2 \neq 0$. When $P_2 = 0$ (before the threshold of P_2 presence), solutions are identical with general NPZD system.

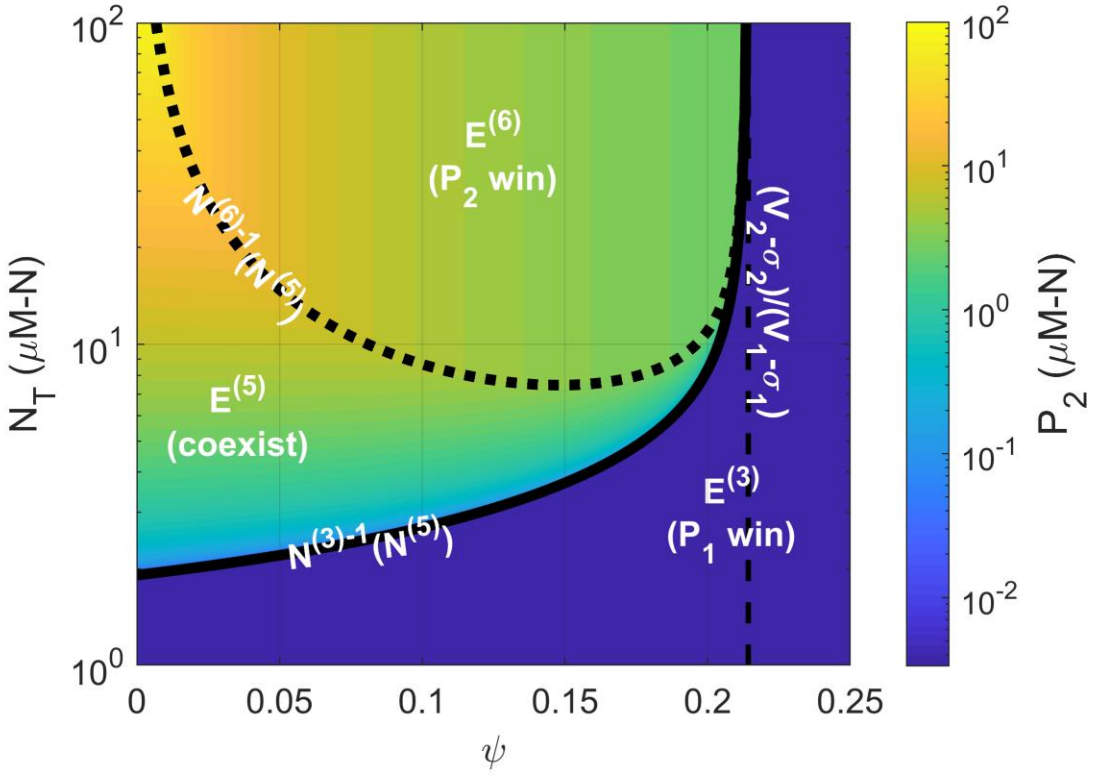

Figure 5. Sensitivity of thresholds for $E^{(5)}$ and $E^{(6)}$ to the coefficient ψ. When $\psi \approx 0$, $E^{(6)}$ is not feasible because the threshold increases infinitely. When ψ is sufficiently large, P_2 cannot survive in the system and only $E^{(3)}$ is feasible.

4. Discussion

4.1. Numerical solutions using ordinary differential equation solver and time scale for P_2 bloom

Figure 6 shows numerical solutions obtained by MATLAB's ordinary differential equation solver (ode45) for different ψ and N_T. The title in each subplot shows the analytically determined condition of the system. When N_T is less than $N^{(3)^{-1}}(N^{(5)})$, numerical solutions

show that P_2 cannot be sustained in the system and converges to zero, whereas P_2 converges to a non-zero constant when condition (5) is satisfied (Figure 6). Similarly, P_1 exponentially decreases and converges to zero when condition (6) is satisfied (Figure 6). When $\psi = 0$, P_2 always coexists with P_1; on the other hand, P_2 is never sustained by the system when $(V_2 - \sigma_2)/(V_1 - \sigma_2) < \psi$, regardless of N_T. The sensitivity of the numerical solution on ψ and N_T matches the theoretical stability condition for equilibriums discussed in section 3.

The numerical solutions also show several features that are not resolved by the equilibrium theory: biogeochemical oscillations and temporal transitions between equilibriums. As mentioned above, equilibriums change from a stable focal point to a neutral stability point when the system is sufficiently eutrophic. The oscillations become stiffer as N_T increases, which cause the system to adjust to the wrong equilibrium that disagrees with the steady-state solution (Appendix A). Several experiments clearly show that the system is initially attracted by $E^{(3)}$ and then slowly moves to equilibriums that include a HAB group, $E^{(5)}$ or $E^{(6)}$. During the initial phase of transition from $E^{(3)}$ to the other equilibriums that include P_2 (with concentration negligible at this stage), the growth rate of P_2 is asymptotically given as

$$\frac{\partial P_2}{\partial t} = \left(U_2\left(N^{(3)}\right) - \frac{\psi}{P_1^{(3)}} GZ^{(3)} - \sigma_2 \right) P_2. \tag{7}$$

which indicates exponential growth of P_2 and the net growth rate of $U_2\left(N^{(3)}\right) - \psi/P_1^{(3)} GZ^{(3)} - \sigma_2$. The reciprocal of the rate given in (7) yields a time scale for the P_2 bloom. As mentioned in section 3.2.2, the growth rate should be positive for the system to be attracted by $E^{(5)}$, and the positivity condition for the growth rate can be written as ${N^{(3)}}^{-1}\left(N^{(5)}\right) < N_T$. Therefore, the growth rate converges to zero as N_T approaches the threshold, so the transition from $E^{(3)}$ to the

equilibriums including P_2 can be slow when N_T is close to the threshold. Figure 7 shows good correlation between the numerical and theoretical time scales of the P_2 bloom. The numerical time scales are subjectively defined from Figure 6 and marked as dashed lines. The theoretical time scales are defined as the reciprocal of the growth rate of P_2 in equation (7).

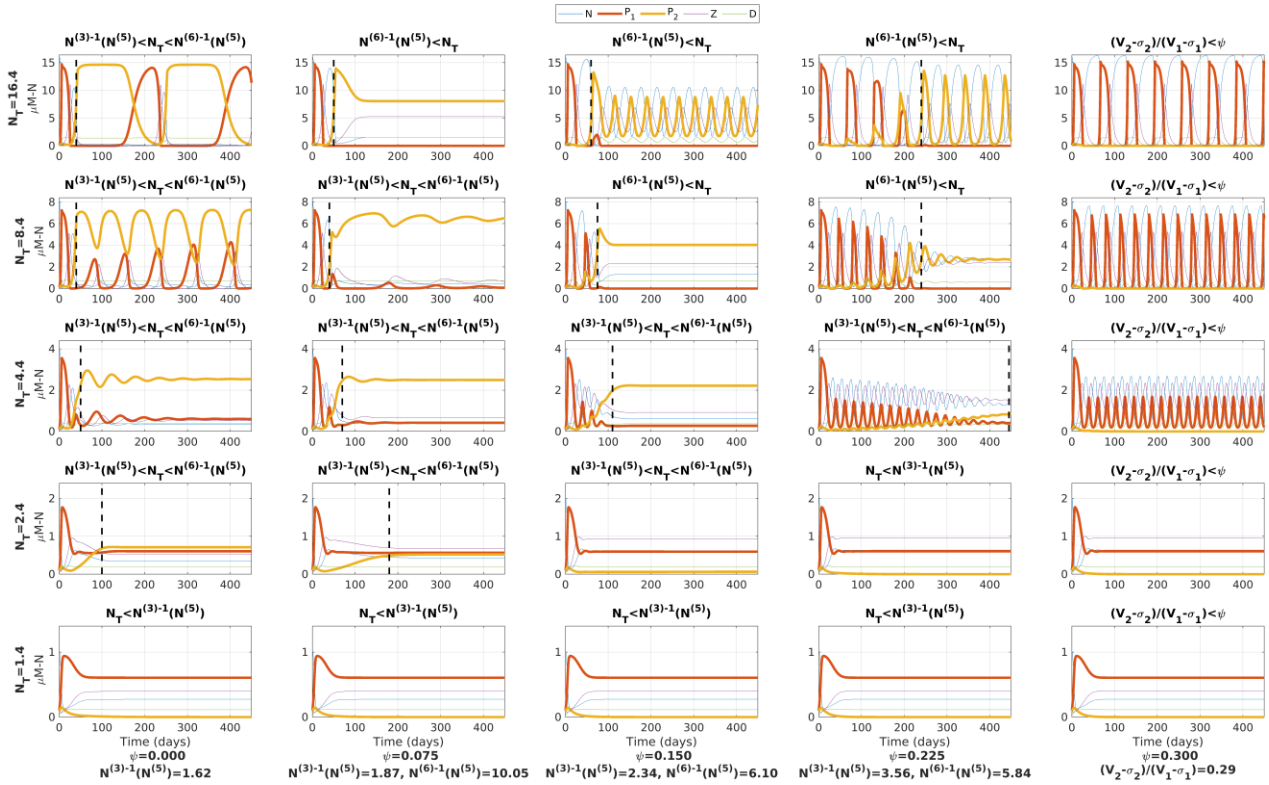

Figure 6. Numerical solutions of system (1) with different total nitrogen concentration N_T and relative predation avoidance ψ. The title of each panel indicates the analytically determined condition of each solution. If $N_T < N^{(3)^{-1}}(N^{(5)})$, P_2 is defeated by P_1 in resource competition. If $N^{(3)^{-1}}(N^{(5)}) < N_T < N^{(6)^{-1}}(N^{(5)})$, both P_1 and P_2 coexist. If $N^{(6)^{-1}}(N^{(5)}) < N_T$, P_1 cannot survive due

to too strong predation pressure. If $\psi = 0$, P_1 always coexists with P_2. If $(V_2 - \sigma_2)/(V_1 - \sigma_1) < \psi$, P_2 cannot survive regardless of N_T. Black dashed lines indicate time scales for the P_2 bloom subjectively determined.

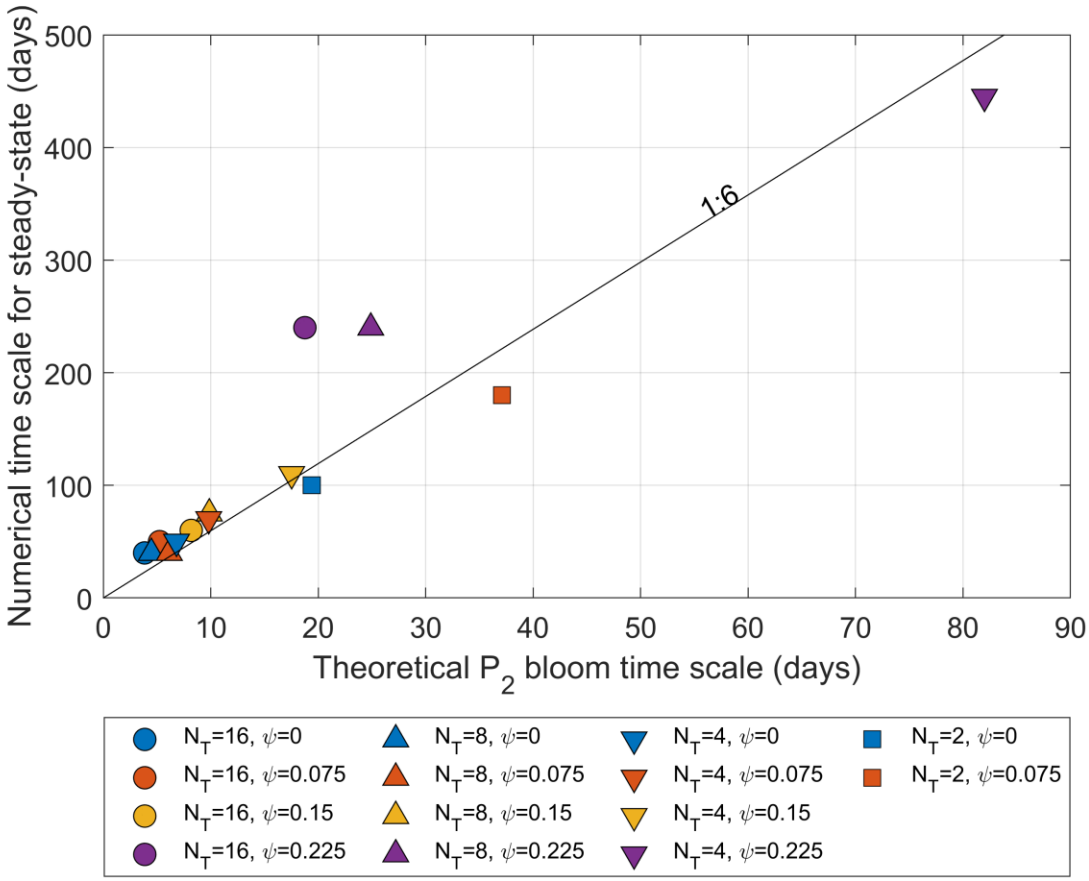

Figure 7. Relation between theoretical time scales for P_2 bloom, defined as the reciprocal of the growth rate in equation (7), and those from the numerical solutions estimated from Figure 6.

4.2. Sensitivity experiments using fully coupled ecosystem model with hydrodynamics model

Figure 8 shows results from the idealized experiments that use the fully coupled ecosystem model with ROMS initiated from nutrient concentration N=1, 4, and 16 μM-N. The theoretical stability condition for equilibrium predicts that the experiment using N=1 μM-N

(upper panels of Figure 8) simulates $E^{(3)}$ where P_1 wins, N=4 μM-N (middle panels of Figure 8) simulates $E^{(5)}$ where both P_1 and P_2 coexist, and N=16 μM-N (lower panels of Figure 8) simulates $E^{(6)}$ where P_2 wins. These results match the numerical simulation results even though the theory does not consider temporal changes of ecological variables, physical transport, and sinking detritus. Figure 9 shows that the concentration of each simulated phytoplankton group is in good agreement with the analytically predicted phytoplankton concentration (red lines in Figure 9) based on the simulated total nitrogen and the steady state solutions found in previous sections.

Figure 10 shows the surface passive tracer and total nitrogen concentration (which have different initial values) of each simulation after 90 days. The distribution of total nitrogen concentration is almost identical to that of a passive tracer that is transported by purely ocean currents and mixed without influence from the biogeochemical processes considered in the ecosystem model. This suggests that total nitrogen is predominantly determined by the physical transport in the coastal and bay regions (which in this case is determined by the tides). The passive tracer concentration in the shallow marginal region of the inner bay is almost identical to the initial condition of the tracer, implying a long residence time. On the other hand, the tracer concentration away from the margins of the inner bay is considerably reduced and transported to the offshore region, indicating a much shorter residence time there. Similarly, total nitrogen concentration is nearly the same as the initial condition in the shallow margins of the bay (yellowish markers in Figure 9) but reduced in regions toward the inlet and coast owing to rapid transport seaward (blueish markers in Figure 9). Therefore, the shallow margins maintain enough total nitrogen to exceed the thresholds for HAB group presence, but the other regions away from the margin cannot (Figures 8 and 9). This behavior of the fully coupled model matches well with

the conceptual model proposed by Smayda (2008). Consequently, physical transport in the shallow tide-dominated coastal bay plays a strong role in determining total nitrogen concentration (Figure 8), after which the response of the ecosystem (in terms of phytoplankton concentration of each group; Figure 9) follows the dynamics described by the equilibriums of the model.

It is worth noting that the idealized experiments are simplified and several physical dynamics that occur in real coastal systems are not resolved (e.g., temporal changes of light intensity, subtidal forcing, wind-driven circulations, river discharges). However, the experiments imply that the dynamics described by the equilibriums can be dominant in complex semi-closed coastal regions with predominant tidal currents, and can be valid when the time scale of the P_2 bloom is shorter than the other unresolved processes.

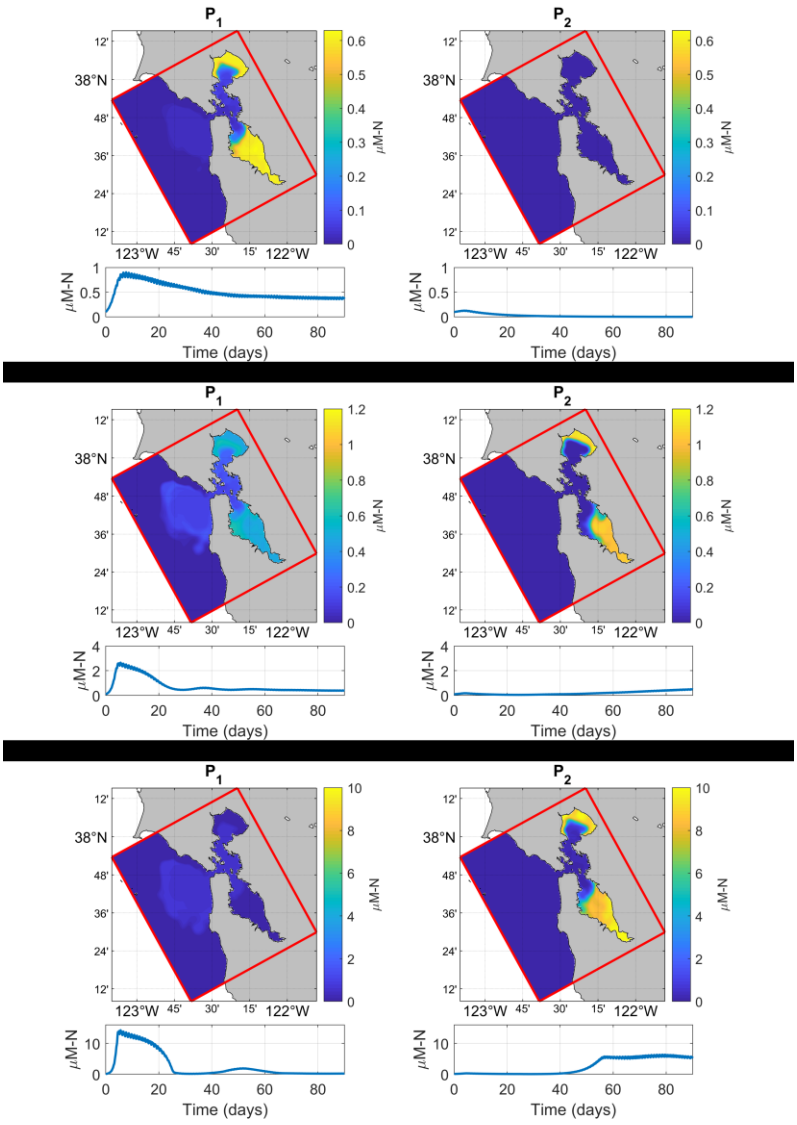

Figure 8. The idealized numerical experiment results where total nitrogen concentration at the inner bay is set to N_T=1.4 (upper panels), 4.4 (middle panels), and 16.4 μM-N(lower panels). Each in turn satisfies $N^{(3)^{-1}}(N^{(5)})$ where P_2 is not sustained, $N^{(3)^{-1}}(N^{(5)}) < N_T < N^{(6)^{-1}}(N^{(5)})$ where both P_1 and P_2 coexist, and $N^{(6)^{-1}}(N^{(5)}) < N$ where P_1 cannot survive. The spatial distribution of the tracers indicates the surface concentration after 90 days. The time series show the spatially averaged phytoplankton concentration at the inner shelf region.

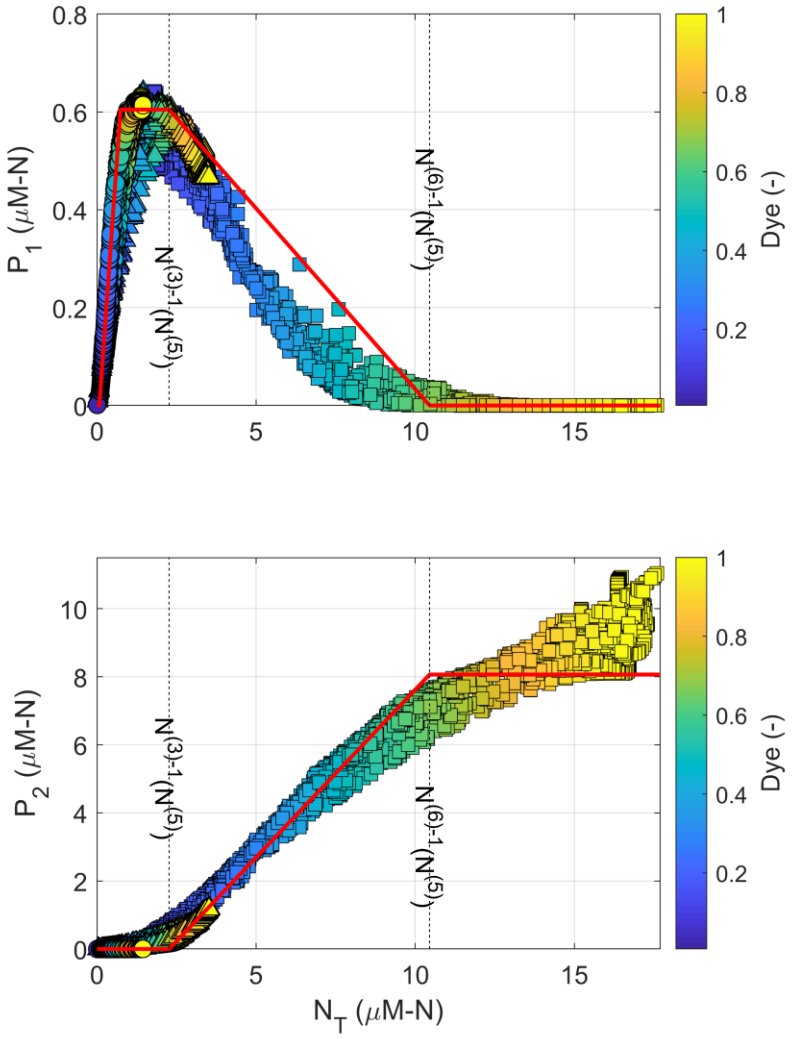

Figure 9. Relation between surface total nitrogen and each phytoplankton group, P_1 (upper panel) and P_2 (lower panel), simulated in the idealized experiments after 90 days at the inner shelf region. Color indicates passive tracer concentration. Red lines indicate analytically calculated phytoplankton concentration using the steady-state solutions and the simulated total nitrogen concentration. Square, triangle, and circle markers indicate each experiment initiated by $N_T =$ 1.4, 4.4, and 16.4 μM-N, respectively.

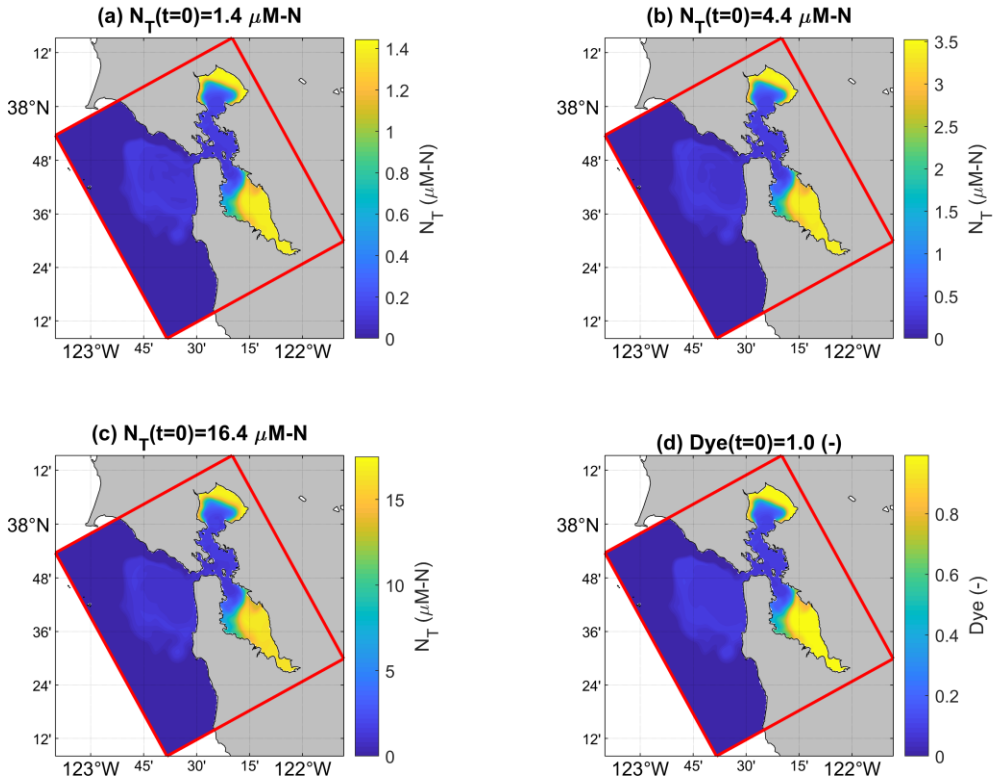

62

63 **Figure 10.** Simulated surface total nitrogen in the numerical experiments initiated by $N_T = 1.4$
64 (a), 4.4 (b), and 16.4 μM-N (c), and passive tracer concentration (d) after 90 days. The total
65 nitrogen concentration has almost identical distribution as the passive tracers, and implies that
66 total nitrogen is determined by physical transport.

67

68 Recently, the importance of resource competition and prey avoidance in HAB dynamics
69 has been suggested by many studies. In particular, prey avoidance is pointed out as a key HAB
70 mechanism for *Heterosigma akashiwo* blooms and also for other cases such as *Isochrysis*
71 *galbana* (Mitra and Flynn, 2006) and *Aureoumbra lagunensis* (Kang et al., 2015) blooms where
72 the dynamics discussed in this study and the fully coupled model are applicable. The systematic

(mathematical) population dynamics of resource competition was analytically examined by Tilman (1977) and is providing surprising insight to problems involving resource competition and coexistence. Although previous field and laboratory studies suggested that prey avoidance can be key mechanism in many HABs cases (Mitra and Flynn, 2006; Harvey and Menden-Deuer, 2011 and 2012; Kang et al., 2015), the population dynamics of prey avoidance was not analytically resolved. Here, the analytical development suggests that the system must be sufficiently eutrophic (enough total nitrogen in the system to exceed a threshold) for HABs to be triggered by prey avoidance. This finding supports modern conceptual models for HABs that show a positive relation between eutrophication and HABs (Smayda, 2008; Gilbert and Burkholder, 2011 and 2018; Griffith and Gobler, 2020). The numerical experiments using the fully coupled model demonstrate that the dynamics discussed by the equilibriums is predominant for a realistic coastal environment governed by strong tides. The relationship between residence time and HABs resolved here matches well with conceptual models for HABs (Smayda, 2008).

The feasible steady-state solutions are transitioned from one to another whenever total nitrogen level N_T in the system is higher than the thresholds determined by model coefficients (Figures 4 and 6). If the ecosystem is not sufficiently eutrophic to sustain enough zooplankton, $N_T < {N^{(3)}}^{-1}\left(N^{(5)}\right)$, the predation of zooplankton is not considerable, and steady-state solutions shared with the traditional NPZD model without a HAB group (i.e., $P_2 = 0$) appear as a consequence of resource competition, with the non-harmful phytoplankton defeating the HAB group. When the ecosystem is sufficiently eutrophic to sustain a large enough zooplankton group, ${N^{(3)}}^{-1}\left(N^{(5)}\right) < N_T < {N^{(6)}}^{-1}\left(N^{(3)}\right)$, zooplankton can sufficiently pump nitrogen from the non-harmful phytoplankton to the nutrient pool, and an equilibrium condition is satisfied resulting in two coexisting phytoplankton groups ($E^{(5)}$). When the ecosystem is excessively eutrophic and a

large zooplankton group can be sustained by the HAB group, $N^{(6)^{-1}}\left(N^{(3)}\right) < N_T$, the HAB group itself can sustain the zooplankton group without P_1 and the predation pressure for P_1 becomes too intense, resulting in a steady-state solution without normal phytoplankton ($E^{(6)}$).

The feasibility of steady-state solutions resulting in HABs is sensitive to the relative HAB group predation avoidance parameter ψ (Figure 5). When $\psi = 0$, a steady-state solution in which the HAB group outperforms the non-harmful phytoplankton group is not feasible because the HAB group cannot sustain the zooplankton group. As ψ increases, the threshold for the solution without non-harmful phytoplankton decreases because the HAB group efficiently sustains the zooplankton, yet the steady-state concentration of the HAB group also decreases with increasing predation. When $\psi > (V_2 - \sigma_2)/(V_1 - \sigma_1)$, both equilibrium conditions supporting HAB growth are not feasible because the HAB group cannot gain an advantage through better predation avoidance. The time scale for the system to move from equilibrium without P_2 to that with P_1 is asymptotically determined and is in good agreement with numerical solutions.

5. Conclusion

In this study, a modified NPZD system that highlights different predation pressure for two phytoplankton functional groups (one harmful and one non-harmful) is described and the possible steady-state solutions are discussed. Analytical solutions show theoretically that increased nitrogen levels from anthropogenic nutrient loading can alter the coastal ecosystem from conditions that cannot trigger HABs to conditions that can (that is, steady state solutions move from one equilibrium state to another). The thresholds may explain the dynamics of regime

shift which alter the dominant species in an ecosystem by favoring the HAB group. Steady state solutions to the coupled ecosystem model reveal details of the top-down control dynamics. Results show that (1) HABs can be suppressed because of resource competition with non-harmful phytoplankton, and (2) HABs having better predation avoidance can be triggered when total nitrogen exceeds a threshold by using nutrients pumped by zooplankton from non-harmful phytoplankton pools.

We expect that the population dynamics of the prey avoidance elucidated by this study (e.g., presence of total nitrogen thresholds for HAB groups having better prey avoidance to overcome defeat in resource competition) can provide insight to better understand field observations, laboratory experiments, and numerical models. The analytical study describes population dynamics between two primal producers that compete for one resource and are influenced by different predation pressure from one zooplankton group. The dynamics are applicable to not only the HABs problem but also any other system with top-down control. The structure of the model (different phytoplankton groups influenced by different predation pressure from one zooplankton group) has frequently been included in various complex ecosystem models. However, the role of the dynamics in the ecosystem and the sensitivity of the parameters controlling relative predation pressure were not considered. This study shows how the different predation pressures on each phytoplankton group change the population of each group, what conditions are required for the plankton group impacted less by predation to be sustained in the ecosystem, and how the ecosystem is influenced by changes to parameters controlling relative predation pressure.

Appendix A: Problem of numerical solutions

Figure A1 shows that the numerical solution using $N_T = 32.4\ \mu M\text{-}N$ and $\psi = 0.15$ satisfies condition (6) where P_1 cannot survive. In this case, equilibrium is not a stable focal point but rather a neutral stability point which causes a stiff biogeochemical oscillation centered on $E^{(6)}$ where there is no P_1. However, numerical solutions show different results which depend on the choice of solvers and error tolerances (Figure A1). We presumed that the solutions that do not sustain P_1 are correct results because theoretically the system must be attracted by $E^{(6)}$ where there is no P_1, and solutions having better accuracy (smaller error tolerance) simulate oscillations without P_2. This result shows that the wrong equilibrium can be reached by the numerical solutions when using low accuracy.

The modified NPZD model fully coupled with ROMS uses a scheme consistent with other ecosystem models already implemented in ROMS: a first order explicit Euler scheme for the processes that increase concentration of state variables, and an implicit Euler scheme for the processes that decrease the concentration. However, it must be noted that this scheme may not be sufficiently accurate to properly simulate highly eutrophic environments attracted by $E^{(6)}$ with stiff oscillations.

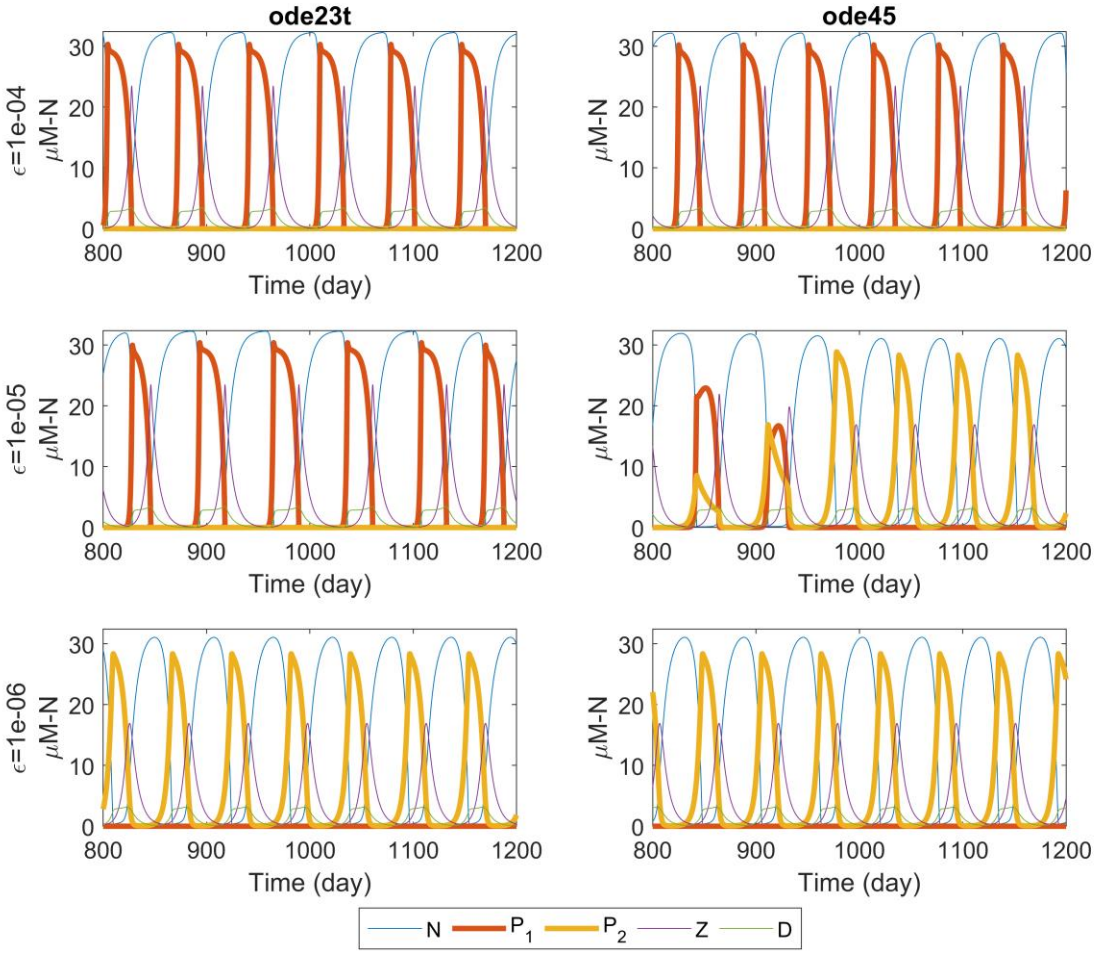

157

158 **Figure A1.** Numerical solution of system (1) with $N_T = 32.4\ \mu M\text{-}N$ and $\psi = 0.15$ that is

159 theoretically attracted by $E^{(6)}$ where there is no P_1. Less accurate solutions, large error tolerances,

160 and ode23t relative to ode45 tend to simulate oscillations where P_1 is dominant.

161

162 **Appendix B: Explicit forms of the thresholds for $P_2 \neq 0$ equilibriums**

163 Explicit forms of the thresholds of $P_2 \neq 0$ steady-state solutions are given as

$$N^{(3)^{-1}}\left(N^{(5)}\right) = \frac{(k_1 + \epsilon_1 + \epsilon_2 - \epsilon_3)^2 - (k_1 + \epsilon_2 - \epsilon_3)^2 + 4k_1\epsilon_2}{4k_1 + 2\epsilon_1}$$

$$N^{(6)^{-1}}\left(N^{(3)}\right) = \frac{(k_2 + \epsilon_1 + \epsilon_2{}' - \epsilon_3{}')^2 - (k_2 + \epsilon_2{}' - \epsilon_3{}')^2 + 4k_1\epsilon_2{}'}{4k_2 + 2\epsilon_1}$$

where

$$\epsilon_1 = \frac{\sqrt{\left((\sigma_2 - \sigma_1\psi)(k_1 + k_2) - V_2k_1 + \psi V_1k_2\right)^2 - 4k_1k_2(\sigma_2 - \psi\sigma_1)\left(\sigma_2 - V_2 - \psi(V_1 - \sigma_1)\right)} - V_2k_1 + (\sigma_2 - \psi\sigma_1)(k_1 + k_2) + \psi V_1k_2}{V_2 - \sigma_2 - (V_1 - \sigma_1)}$$

$$\epsilon_2 = \frac{1}{\Lambda}\ln\left[\left(1 + \frac{\xi}{R_m(\gamma - 1)}\right)^{-1}\psi\right]\left(\frac{\sigma_1(\gamma - 1)}{\xi} + \frac{\gamma\sigma_1}{\delta} + 1\right)$$

$$\epsilon_2' = \frac{1}{\psi\Lambda}\ln\left[\left(1 + \frac{\xi}{R_m(\gamma - 1)}\right)^{-1}\right]\left(\frac{\sigma_2(\gamma - 1)}{\xi} + \frac{\gamma\sigma_2}{\delta} + 1\right)$$

$$\epsilon_3 = \frac{1}{\Lambda}\ln\left[\left(1 + \frac{\xi}{R_m(\gamma - 1)}\right)^{-1}\right]V_1(\gamma - 1)\left(\frac{1}{\delta} + \frac{1}{\xi}\right)$$

$$\epsilon_3' = \frac{1}{\psi\Lambda}\ln\left[\left(1 + \frac{\xi}{R_m(\gamma - 1)}\right)^{-1}\right]V_2(\gamma - 1)\left(\frac{1}{\delta} + \frac{1}{\xi}\right).$$

Acknowledgement

This work was supported by funds from the University of New Hampshire and NSF Physical Oceanography grant number OCE1459609. Jang-Geun Choi is partly supported by the U.S. Department of Energy's Office of Energy Efficiency and Renewable Energy (EERE) under the Water Power Technology Office (WPTO) Award Number DE-EE0009450 and NSF EPSCoR Project entitled "Towards tracking organic carbon cycling in a changing Arctic Ocean".

Data availability statement

The modified NPZD ecosystem model fully coupled with ROMS in this study is available at https://github.com/Jang-Geun/roms_nppzd_psi.

References

Anderson, D.M., 2009. Approaches to monitoring, control and management of harmful algal blooms (HABs). Ocean Coast. Manag. 52, 342–347. https://doi.org/10.1016/J.OCECOAMAN.2009.04.006

Baek, S.H., Kim, Y., Lee, M., Ahn, C.-Y., Cho, K.H., Park, B.S., 2020. Potential Cause of Decrease in Bloom Events of the Harmful Dinoflagellate Cochlodinium polykrikoides in Southern Korean Coastal Waters in 2016. Toxins (Basel). 12, 390. https://doi.org/10.3390/toxins12060390

Busenberg, S., Kumar, S.K., Austin, P., Wake, G., 1990. The dynamics of a model of a plankton-nutrient interaction. Bull. Math. Biol. 52, 677–696. https://doi.org/10.1007/BF02462105

Cho, H.-Y., Cho, B.J., 2014. Optimal Growth Model of the Cochlodinium Polykrikoides. J. Korean Soc. Coast. Ocean Eng. 26, 217–224.

Cruz-Rico, J., Rivas, D., 2018. Physical and biogeochemical variability in Todos Santos Bay, northwestern Baja California, derived from a numerical NPZD model. J. Mar. Syst. 183, 63–75. https://doi.org/10.1016/j.jmarsys.2018.04.001

193 Cullen, J.J., Franks, P.J.S., Karl, D.M., Longhurst, A., 2002. Physical influences on marine
194 ecosystem dynamics, in: Robinson, A.R., McCarthy, J.J., Rothschild, B.J. (Eds.), The Sea,
195 Biological-Physical Interactions in the Sea. Wiley, pp. 297–336.

196 Edwards, A.M., 2001. Adding Detritus to a Nutrient-Phytoplankton-Zooplankton Model: A
197 Dynamical-Systems Approach. J. Plankton Res. 23, 389–413.
198 https://doi.org/10.1093/plankt/23.4.389

199 Eppley, R.W., Rogers, J.N., McCarthy, J.J., 1969. Half-saturation constants for uptake of nitrate
200 and ammonium by marine phytoplankton. Limnol. Oceanogr. 14, 912–920.
201 https://doi.org/10.4319/LO.1969.14.6.0912

202 Fennel, K., Wilkin, J., Levin, J., Moisan, J., O'Reilly, J., Haidvogel, D., 2006. Nitrogen cycling
203 in the Middle Atlantic Bight: Results from a three-dimensional model and implications for
204 the North Atlantic nitrogen budget. Global Biogeochem. Cycles 20.
205 https://doi.org/10.1029/2005GB002456

206 Fennel, W., Neumann, T., 2004. Introduction to the Modelling of Marine Ecosystems. Elsevier.

207 Fiechter, J., Moore, A.M., Edwards, C.A., Bruland, K.W., Di Lorenzo, E., Lewis, C.V.W.,
208 Powell, T.M., Curchitser, E.N., Hedstrom, K., 2009. Modeling iron limitation of primary
209 production in the coastal Gulf of Alaska. Deep. Res. Part II Top. Stud. Oceanogr. 56, 2503–
210 2519. https://doi.org/10.1016/j.dsr2.2009.02.010

Fistarol, G.O., Legrand, C., Selander, E., Hummert, C., Stolte, W., Granéli, E., 2004. Allelopathy in Alexandrium spp.: effect on a natural plankton community and on algal monocultures. Aquat. Microb. Ecol. 35, 45–56. https://doi.org/10.3354/ame035045

Flynn, K.J., 2008. Attack is not the best form of defense: Lessons from harmful algal bloom dynamics. Harmful Algae 8, 129–139. https://doi.org/10.1016/J.HAL.2008.08.007

Glibert, P.M., Burkholder, J.M., 2011. Harmful algal blooms and eutrophication: "strategies" for nutrient uptake and growth outside the Redfield comfort zone. Chinese J. Oceanol. Limnol. 29, 724–738. https://doi.org/10.1007/S00343-011-0502-Z

Glibert, P.M., Burkholder, J.M., 2018. Causes of Harmful Algal Blooms, in: Shumway, S.E., Burkholder, J.M., Morton, S.L. (Eds.), Harmful Algal Blooms: A Compendium Desk Reference. Wiley Blackwell, pp. 1–38.

Griffith, A.W., Gobler, C.J., 2020. Harmful algal blooms: A climate change co-stressor in marine and freshwater ecosystems. Harmful Algae. https://doi.org/10.1016/j.hal.2019.03.008

Harvey, E.L., Menden-Deuer, S., 2012. Predator-induced fleeing behaviors in phytoplankton: a new mechanism for harmful algal bloom formation? PLoS One 7. https://doi.org/10.1371/JOURNAL.PONE.0046438

Harvey, E.L., Menden-Deuer, S., 2011. Avoidance, movement, and mortality: The interactions between a protistan grazer and Heterosigma akashiwo, a harmful algal bloom species. Limnol. Oceanogr. 56, 371–378. https://doi.org/10.4319/LO.2011.56.1.0371

He, R., McGillicuddy, D.J., Keafer, B.A., Anderson, D.M., 2008. Historic 2005 toxic bloom of Alexandrium fundyense in the western Gulf of Maine: 2. Coupled biophysical numerical modeling. J. Geophys. Res. Ocean. 113, 7040. https://doi.org/10.1029/2007JC004602

Heinle, A., Slawig, T., 2013. Impact of parameter choice on the dynamics of NPZD type ecosystem models. Ecol. Modell. 267, 93–101. https://doi.org/10.1016/j.ecolmodel.2013.07.019

Heinle, A., Slawig, T., 2013. Internal dynamics of NPZD type ecosystem models. Ecol. Modell. 254, 33–42. https://doi.org/10.1016/j.ecolmodel.2013.01.012

Jeong, H.J., Lim, A.S., Lee, K., Lee, M.J., Seong, K.A., Kang, N.S., Jang, S.H., Lee, K.H., Lee, S.Y., Kim, M.O., Kim, J.H., Kwon, J.E., Kang, H.C., Kim, J.S., Yih, W., Shin, K., Jang, P.K., Ryu, J.-H., Kim, S.Y., Park, J.Y., Kim, K.Y., Jeong, H.J., Lim, A.S., Lee, K., Lee, M.J., Seong, K.A., Kang, N.S., Jang, S.H., Lee, K.H., Lee, S.Y., Kim, M.O., Kim, J.H., Kwon, J.E., Kang, H.C., Kim, J.S., Yih, W., Shin, K., Jang, P.K., Ryu, J.-H., Kim, S.Y., Park, J.Y., Kim, K.Y., 2017. Ichthyotoxic Cochlodinium polykrikoides red tides offshore in the South Sea, Korea in 2014: I. Temporal variations in three-dimensional distributions of red-tide organisms and environmental factors. Algae 32, 101–130. https://doi.org/10.4490/ALGAE.2017.32.5.30

Jeong, H.J., Shim, J.H., Kim, J.S., Park, J.Y., Lee, C.W., Lee, Y., 1999. Feeding by the mixotrophic thecate dinoflagellate Fragilidium cf. mexicanum on red-tide and toxic dinoflagellates. Mar. Ecol. Prog. Ser. 176, 263–277. https://doi.org/10.3354/meps176263

Jeong, H.J., Yoo, Y. Du, Kim, J.S., Kim, T.H., Kim, J.H., Kang, N.S., YIH, W., 2004. Mixotrophy in the Phototrophic Harmful Alga Cochlodinium polykrikoides (Dinophycean): Prey Species, the Effects of Prey Concentration, and Grazing Impact. J. Eukaryot. Microbiol. 51, 563–569. https://doi.org/10.1111/j.1550-7408.2004.tb00292.x

Jin, D., Thunberg, E., Hoagland, P., 2008. Economic impact of the 2005 red tide event on commercial shellfish fisheries in New England. Ocean Coast. Manag. 51, 420–429. https://doi.org/10.1016/j.ocecoaman.2008.01.004

Kang, Y., Koch, F., Gobler, C.J., 2015. The interactive roles of nutrient loading and zooplankton grazing in facilitating the expansion of harmful algal blooms caused by the pelagophyte, Aureoumbra lagunensis, to the Indian River Lagoon, FL, USA. Harmful Algae 49, 162–173. https://doi.org/10.1016/J.HAL.2015.09.005

Kim, D.W., Jo, Y.H., Choi, J.K., Choi, J.G., Bi, H., 2016. Physical processes leading to the development of an anomalously large Cochlodinium polykrikoides bloom in the East sea/Japan sea. Harmful Algae 55, 250–258. https://doi.org/10.1016/j.hal.2016.03.019

Kishi, M.J., Kashiwai, M., Ware, D.M., Megrey, B.A., Eslinger, D.L., Werner, F.E., Noguchi-Aita, M., Azumaya, T., Fujii, M., Hashimoto, S., Huang, D., Iizumi, H., Ishida, Y., Kang, S., Kantakov, G.A., Kim, H. cheol, Komatsu, K., Navrotsky, V. V., Smith, S.L., Tadokoro, K., Tsuda, A., Yamamura, O., Yamanaka, Y., Yokouchi, K., Yoshie, N., Zhang, J., Zuenko, Y.I., Zvalinsky, V.I., 2007. NEMURO-a lower trophic level model for the North Pacific marine ecosystem. Ecol. Modell. 202, 12–25. https://doi.org/10.1016/j.ecolmodel.2006.08.021

Koné, V., Machu, E., Penven, P., Andersen, V., Garçon, V., Fréon, P., Demarcq, H., 2005. Modeling the primary and secondary productions of the southern Benguela upwelling system: A comparative study through two biogeochemical models. Global Biogeochem. Cycles 19. https://doi.org/10.1029/2004GB002427

Kudela, R.M., Seeyave, S., Cochlan, W.P., 2010. The role of nutrients in regulation and promotion of harmful algal blooms in upwelling systems. Prog. Oceanogr. 85, 122–135. https://doi.org/10.1016/J.POCEAN.2010.02.008

Kwon, H.-K., Kim, H.-J., Yang, H.-S., Oh, S.-J., 2014. Non-Outbreak Cause of Cochlodinium Bloom in the Western Coast of Jaran Bay in Summer, 2013 : On the Basis of Nutrient Data. J. Korean Soc. Mar. Environ. Saf. 20, 372–381. https://doi.org/10.7837/kosomes.2014.20.4.372

Lee, C.K., Kim, H.C., Lee, S.-G., Jung, C.S., Kim, H.G., Lim, W.A., 2001. Abundance of harmful algae, Cochlodinium polykrikoides, Gyrodinium impudicum and Gymnodinium catenatum in the coastal area of South Sea of Korea and their effects of temperature, salinity, irradiance and nutrient on the growth in culture. Korean J. Fish. Aquat. Sci. 34, 536–544.

Lee, C.K., Park, T.G., Park, Y.T., Lim, W.A., 2013. Monitoring and trends in harmful algal blooms and red tides in Korean coastal waters, with emphasis on Cochlodinium polykrikoides. Harmful Algae 30, S3–S14. https://doi.org/10.1016/j.hal.2013.10.002

Lee, D.K., 2008. Cochlodinium polykrikoides blooms and eco-physical conditions in the South Sea of Korea. Harmful Algae 7, 318–323. https://doi.org/10.1016/j.hal.2007.12.014

Li, Y., He, R., McGillicuddy, D.J., Anderson, D.M., Keafer, B.A., 2009. Investigation of the 2006 Alexandrium fundyense bloom in the Gulf of Maine: In-situ observations and numerical modeling. Cont. Shelf Res. 29, 2069–2082. https://doi.org/10.1016/J.CSR.2009.07.012

Lim, A.S., Jeong, H.J., Jang, T.Y., Jang, S.H., Franks, P.J.S., 2014. Inhibition of growth rate and swimming speed of the harmful dinoflagellate Cochlodinium polykrikoides by diatoms: Implications for red tide formation. Harmful Algae 37, 53–61. https://doi.org/10.1016/j.hal.2014.05.003

Lima, I.D., Doney, S.C., 2004. A three-dimensional, multinutrient, and size-structured ecosystem model for the North Atlantic. Global Biogeochem. Cycles 18. https://doi.org/10.1029/2003GB002146

Margalef, R., 1978. Life-forms of phytoplankton as survival alternatives in an unstable environment. Oceanol. acta 1, 493–509.

Mellor, G.L., Yamada, T., 1982. Development of a turbulence closure model for geophysical fluid problems. Rev. Geophys. 20, 851–875. https://doi.org/10.1029/RG020I004P00851

Mitra, A., Flynn, K.J., 2006. Promotion of harmful algal blooms by zooplankton predatory activity. Biol. Lett. 2, 194–197. https://doi.org/10.1098/rsbl.2006.0447

Newberger, P.A., Allen, J.S., Spitz, Y.H., 2003. Analysis and comparison of three ecosystem models. J. Geophys. Res. Ocean. 108. https://doi.org/10.1029/2001jc001182

311 Oguz, T., Mourre, B., Tintoré, J., 2016. Upstream control of the frontal jet regulating plankton
312 production in the Alboran Sea (Western Mediterranean). J. Geophys. Res. Ocean. 121,
313 7159–7175. https://doi.org/10.1002/2016JC011667

314 Oh, S.J., Kim, H.J., Kwon, H.K., Yang, H.-S., Kim, S.Y., 2015. Effect of Nutrients on
315 Competition among the Harmful Dinoflagellates Cochlodinium polykrikoides and the
316 Diatom Skeletonema sp. in Jaran Bay Using a Mathematical Model. Sea 20, 92–101.
317 https://doi.org/10.7850/jkso.2015.20.2.92

318 Onitsuka, G., Yanagi, T., Yoon, J.-H., 2007. A numerical study on nutrient sources in the surface
319 layer of the Japan Sea using a coupled physical-ecosystem model. J. Geophys. Res. 112,
320 C05042. https://doi.org/10.1029/2006JC003981

321 Padmakumar, K.B., Menon, N.R., Sanjeevan, V.N., 2012. Is Occurrence of Harmful Algal
322 Blooms in the Exclusive Economic Zone of India on the Rise? Int. J. Oceanogr. 1–7.
323 https://doi.org/10.1155/2012/263946

324 Park, T.G., Lim, W.A., Park, Y.T., Lee, C.K., Jeong, H.J., 2013. Economic impact, management
325 and mitigation of red tides in Korea. Harmful Algae 30, S131–S143.
326 https://doi.org/10.1016/j.hal.2013.10.012

327 Perruche, C., Rivière, P., Pondaven, P., Carton, X., 2010. Phytoplankton competition and
328 coexistence: Intrinsic ecosystem dynamics and impact of vertical mixing. J. Mar. Syst. 81,
329 99–111. https://doi.org/10.1016/j.jmarsys.2009.12.006

Post, D.M., Conners, M.E., Goldberg, D.S., 2000. Prey preference by a top predator and the stability of linked food chains. Ecology 81, 8–14. https://doi.org/10.1890/0012-9658

Powell, T.M., Lewis, C.V.W., Curchitser, E.N., Haidvogel, D.B., Hermann, A.J., Dobbins, E.L., 2006. Results from a three-dimensional, nested biological-physical model of the California Current System and comparisons with statistics from satellite imagery. J. Geophys. Res. 111, C07018. https://doi.org/10.1029/2004JC002506

Priester, C.R., Melbourne-Thomas, J., Klocker, A., Corney, S., 2017. Abrupt transitions in dynamics of a NPZD model across Southern Ocean fronts. Ecol. Modell. 359, 372–382. https://doi.org/10.1016/j.ecolmodel.2017.05.030

Shankar, S., Townsend, D.W., Thomas, M.A., 2014. Ammonium and maintenance of bloom populations of Alexandrium fundyense in the Gulf of Maine and on Georges Bank: results of laboratory culture experiments. Mar. Ecol. Prog. Ser. 507, 57–67. https://doi.org/10.3354/MEPS10853

Shchepetkin, A.F., McWilliams, J.C., 2005. The regional oceanic modeling system (ROMS): A split-explicit, free-surface, topography-following-coordinate oceanic model. Ocean Model. 9, 347–404. https://doi.org/10.1016/j.ocemod.2004.08.002

Smayda, T.J., 2008. Complexity in the eutrophication–harmful algal bloom relationship, with comment on the importance of grazing. Harmful Algae 8, 140–151. https://doi.org/10.1016/J.HAL.2008.08.018

Solé, J., Garcia-Ladona, E., Estrada, M., 2006. The role of selective predation in harmful algal blooms. J. Mar. Syst. 62, 46–54. https://doi.org/10.1016/J.JMARSYS.2006.04.002

Sukenik, A., Kaplan, A., 2021. Cyanobacterial harmful algal blooms in aquatic ecosystems: a comprehensive outlook on current and emerging mitigation and control approaches. Microorganisms 9, 1472. https://doi.org/10.3390/MICROORGANISMS9071472

Tang, Y.Z., Gobler, C.J., 2010. Allelopathic effects of Cochlodinium polykrikoides isolates and blooms from the estuaries of Long Island, New York, on co-occurring phytoplankton. Mar. Ecol. Prog. Ser. 406, 19–31. https://doi.org/10.3354/meps08537

Tilman, D., 1977. Resource Competition between Plankton Algae: An Experimental and Theoretical Approach. Ecology 58, 338–348. https://doi.org/10.2307/1935608

van Opheusden, J.H.J., Hemerik, L., van Opheusden, M., van der Werf, W., 2015. Competition for resources: complicated dynamics in the simple Tilman model. Springerplus 4, 1–31. https://doi.org/10.1186/s40064-015-1246-6

Wilkerson, F.P., Dugdale, R.C., Hogue, V.E., Marchi, A., 2006. Phytoplankton blooms and nitrogen productivity in San Francisco Bay. Estuaries and Coasts 29, 401–416. https://doi.org/10.1007/BF02784989/METRICS

Wu, H., Zhu, J., 2010. Advection scheme with 3rd high-order spatial interpolation at the middle temporal level and its application to saltwater intrusion in the Changjiang Estuary. Ocean Model. 33, 33–51. https://doi.org/10.1016/J.OCEMOD.2009.12.001

368 Xu, Q., Lin, H., Liu, Y., Lv, X., Cheng, Y., 2008. Data assimilation in a coupled physical-
369 biological model for the Bohai Sea and the Northern Yellow Sea. Mar. Freshw. Res. 59,
370 529. https://doi.org/10.1071/MF07144

371 Zhou, Y., Zhang, Y., Li, F., Tan, L., Wang, J., 2017. Nutrients structure changes impact the
372 competition and succession between diatom and dinoflagellate in the East China Sea. Sci.
373 Total Environ. 574, 499–508. https://doi.org/10.1016/j.scitotenv.2016.09.092

374